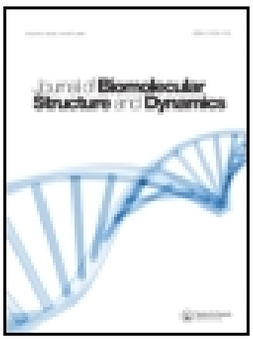

Taylor & Francis
Taylor & Francis Group

Journal of Biomolecular Structure and Dynamics

ISSN: 0739-1102 (Print) 1538-0254 (Online) Journal homepage: http://www.tandfonline.com/loi/tbsd20

Theoretical Investigations and density functional theory based probe of the affinity interaction of saccharide ligands with extra-cellular sialic acid residues

Anjali Patel, Sanjay Tiwari & Prafulla K Jha

To cite this article: Anjali Patel, Sanjay Tiwari & Prafulla K Jha (2018): Theoretical Investigations and density functional theory based probe of the affinity interaction of saccharide ligands with extra-cellular sialic acid residues, Journal of Biomolecular Structure and Dynamics, DOI: 10.1080/07391102.2018.1461690

To link to this article: https://doi.org/10.1080/07391102.2018.1461690

Publisher: Taylor & Francis
Journal: *Journal of Biomolecular Structure and Dynamics*
DOI: http://doi.org/10.1080/07391102.2018.1461690

Theoretical Investigations and density functional theory based probe of the affinity interaction of saccharide ligands with extra-cellular sialic acid residues

Anjali Patel[1], Sanjay Tiwari[2,*] and Prafulla K Jha[1,*]

[1]Department of Physics, Faculty of Science, The Maharaja Sayajirao University of Baroda, Vadodara- 390 002, Gujarat, India
[2]UKA Tarsadia University, Maliba Pharmacy College, Gopal-Vidyanagar Campus, Surat, 394350, Gujarat, India
[*]Email: tiwarisanju@gmail.com, prafullaj@yahoo.com

Abstract

Changes in glycosylation pattern leads to malignant transformations among the cells. In combination with upregulated actions of sialyltransferases, it ultimately leads to differential expression of sialic acid (SA) at cell surface. Given its negative charge and localization to extracellular domain, SA has been exploited as a target for the development of targeted theranostics using approaches, such as, cationization and appending recognition saccharides on carrier surface. In this study, we have performed quantum mechanical calculations based on density functional theory (DFT) to study the interaction of saccharides with extracellular SA. Gradient-corrected DFT with the three parameter function (B3) was utilized for the calculation of Lee-Yang-Parr (LYP) correlation function. Atomic charge, vibrational frequencies and energy of the optimized structures were calculated through B3LYP. Our calculations demonstrate a stronger galactose-sialic acid interaction at tumor-relevant low pH and hyperthermic condition. These results support the application of pH responsive delivery vehicles and targeted hyperthermic chemotherapy for eradicating solid tumor deposits. These studies, conducted *a priori*, can guide the formulation scientists over appropriate choice of ligands and their applications in the design of 'smart' theranostic tools.

Keywords: Cancer; Hypersialylation; Recognition saccharides; Density functional theory;

Targeted theranostics.

List of Abbreviations: SA, sialic acid; DFT, density functional theory; B3LYP, Becke 3-Parameter Lee, Yang and Parr; CMAS, cytidine monophosphate N-acetylneuraminic acid synthase; Gal, galactose; Man, mannose; PBA, phenylboronic acid; DFT, density functional theory; ASDase, aspartate semialdehyde dehydrogenase; $EcPLA_2$, Echis carinatus Phospholipase A_2; AChE, Acetylcholine Esterase; BACE1, Beta-secretase 1; CK2, casein kinase 2; GSK3β, glycogen synthase kinase 3β; BSSE, basis set superposition error; FF, fukui function; NBO, natural bond orbital; HOMO, highest occupied molecular orbital; LUMO, lowest unoccupied molecular orbital; HLG, HOMO-LUMO gap; MEP, molecular electrostatic potential; NC, nanocarriers.

Introduction:

Cell surface proteins are elaborated with covalently attached complex array of N-linked glycans. Glycans offer correct folding of the protein, provide resistance to proteases and facilitate its interaction with ligands. Changes in glycosylation pattern often lead to malignant transformations among the cells (Redondo, Nakamura, De Souza, & Morgado-Diaz, 2004; Guo, Nairn, Harris, Randolph, Alvarez-Manilla et. al., 2008; Hakomori, 2002). This is characterized by an increased branching of N-linked glycans thus creating additional sites for terminal sialic acid (SA) residues. In conjunction with upregulated sialyltransferases, it ultimately leads to hyper-sialylation at cell surface (Kim & Varki, 1997). Furthermore, SA occurs in many tumor-associated carbohydrate antigens, such as, sialylatedTn antigen and sialyl Lewis X and its anti-adhesive characteristics offer a mechanism for cancer cells to detach from a primary tumour and initiate metastasis (Fukuda, 1996). A recent study has demonstrated the association between tumour progression and aberrant sialylation at transcriptional level (Kohnz, Roberts, DeTomaso, Bideyan, Yan et. al., 1996). Moreover, it is shown that over-expression of SA on malignant colonic cells and tissues, in vitro, correlates with the metastatic stage (Azab, Kleinstern, Srebnik, & Rubinstein, 2008).

Given the negative charge, localization to extracellular domain and profound over-expression in cancer cells, SA has been exploited as a target for the development of targeted theranostics. It enables improved screening and focused therapy at the tumour site, thus minimizing adverse events and improving the efficacy of cytotoxic drugs (Bloch, Yavin, Nissan, Ariel, Kenett et. al., 2017; Tiwari, Tirosh, & Rubinstein, 2017). Comprehensive investigations have been conducted using the approaches, such as, cationization (Azab et. al., 2008; Bloch, Kam, Yavin, Moradov, Nissan, et. al., 2012) and appending recognition saccharides (Wang, Wen, Wang, Ma, & Liu, 2017; Wang, Yin, Wang, Shen, Zhu et. al., 2016) and boronated sugar-mimetics (Deshayes, Cabral, Ishii, Miura, Kobayashi et. al., 2013; Lee, Chung, Cho, & Kim 2015) over the carrier surface. Our recent study verifies the dual approach of cationization and attachment of a recognition peptide in the targeting of colon cancer cells, exhibiting metastatic-stage dependent expression of SA. Treatment of cells with neuraminidase resulted into significant decline in the cellular uptake of nanoparticles, thus discerning a definitive role of over-expressed SA in the cell-nanoparticle interaction (Tiwari et. al., 2017).

Experimental evidences suggest that the carriers decorated with saccharides (Wang et. al., 2016) and sugar-mimetics (Deshayes et. al., 2013; Wang, Wu, Zhang, Wang, Qian et. al., 2014) exhibit high affinity towards over-expressed SA and galectin residues on cancer cell surface (Azab et. al., 2008; David, Kopeckova, Kopecek, & Rubinstein, 2002; Varki & Varki, 2007). Still, there is a dearth of supportive theoretical reports exploring these interactions. In the present work, we have focussed our efforts in investigating the comparative interaction of SA with two saccharides (galactose, Gal; mannose, Man) and one sugar-mimetic molecule (phenylboronic acid, PBA) through the state of art density functional theory calculation. Recently, atomistic simulations using density functional theory has become applicable to chemical reaction for the prediction or interpretation of complex behaviour at an atomic level. DFT is preferred for dealing with the several atoms and when a quite accuracy is needed. In the last few decades this type of interaction has been studied extensively using DFT. The

studies on interaction between the nitride based inhibitors and catalytic triad of the Cathepsin K. (Pitchumani Violet Mary, Shankar, & Vijayakumar, 2018; Quesne, Ward, & de Visser, 2013), aspartate semialdehyde dehydrogenase (ASDase) and Amino acid residues Arg103, Asn133, Cys134, Gln161, Ser164, Lys218, Arg239, His246 and Asn321 (Prabhu, Rajamanikandan, Amala, Kanagarajan, & Jeyakanthan, 2018), Piperine and Echis carinatus Phospholipase A_2 ($EcPLA_2$) (Christian Bharathi, Srinivas, & Syed Ibrahim, 2018), Acetylcholine Esterase (AChE) and residues of several ligands Asp72, Trp84, Tyr121, Ser122, Ser200, Trp279, Glu327, Phe330, Phe331, Tyr334, and His440 (Mohammadi & Ghayeb, 2018), Beta-secretase 1 (BACE1) inhibitors and anti P-glycoprotein (Manoharan, Chennoju, & Ghoshal, 2018), Hit15 and casein kinase 2 (CK2) and glycogen synthase kinase 3β (GSK3β) (Pardhi & Vasu, 2018) provides the efficiency of interaction and inhibition using theoretical methods based on DFT. As far as the interaction between SA and Saccharide is concerned very few reports are available (Regueiro-Figueroa, Djanashvili, Esteban-Gómez, de Blas, Platas-Iglesias, & Rodríguez-Blas, 2010; Tanaka, Goi, Tanaka, & Fukase, 2007). Their studies confirmed strong binding between SA and D- galactose at body temperature. However, the pH effect and temperature variation was neglected. We have attempted to outline how such simulation data with varying temperature and pH (Bochevarov, Watson, Greenwood, & Philipp, 2016) may be used as a tool to elaborate the question of ligand interaction with SA as the target and to evaluate if our observations reasonably reproduce the experimental findings. Several studies have shown the possibility to accurately compute pH using approaches based on either quantum mechanics or cheminformatics. (Liptak & Shields, 2001) and thus simulating conformational changes in the ligand-target binding in response to cancer-associated physiological changes. A careful interpretation of our studies can guide the formulation scientists over appropriate choice of ligands and their applications in the design of 'smart' theranostic tools.

Computational Details:

Optimized structures of SA with single and bi-antennary Gal, Man and PBA, interaction of SA with Gal, Man and PBA and the resulting orbital energy calculations were performed by density functional theory (DFT). Gradient-corrected DFT with the three parameter function (B3) was utilized for the calculation of Lee-Yang-Parr (LYP) correlation function (Lee, Yang, & Parr, 1998). Structural parameters were optimized by 6-31G basis set using GAUSSIAN 09 package (Frisch, Trucks, Schlegel, Scuseria, Robb et. al., 2016). B3LYP was used for the calculation of molecular orbital structure, atomic charge, vibrational frequencies and energy of the optimized structures. Further, optimized structural parameters covering the effect of microenvironment pH and temperature were carried out by Jaguar tool of Schrödinger suits program (Trial Version 4.7) (MS Jaguar, 2017). Prior to performing computations, individual molecular structures were placed at a close distance, and allowed to relax under zero external stress and ideal unconstrained conditions. Binding parameters were then obtained from the optimized molecular geometry. Basis set superposition error (BSSE) of intermolecular potential function was corrected by Boys-Bernardi counterpoise method (Boys & Bernardi, 1970). While reduction in the free energy of SA-ligand complex was evaluated as average free energy difference between the bound and unbound states. Interaction energy (E_{int}^{AB}) of ligand-target binding was calculated as the difference between the energy of complex and sum of the energies of its total fragments [Equation 1]:

$$E_{int}^{AB} = E_{AB}^{opt} - (E_{A}^{opt} + E_{B}^{opt}) + E_{AB}^{BSSE} \quad [1]$$

Where, E_{AB}^{opt}, E_{A}^{opt}, E_{B}^{opt} and E_{AB}^{BSSE} are complex energy, ligand energy, receptor energy and BSSE correction respectively.

Fukui function (FF), a predictor of chemical condensed reactivity, specifies the ionization potential and electron affinity (nucleophilicity versus electrophilicity) was calculated as follows (Roy, Usha, Paulovic, & Hirao, 2005) :

$$f^{+}(r) = \rho N + 1(r) - \rho N(r) \quad \text{(Nucleophilic attack)} \quad [2]$$

$$f^{-}(r) = \rho N(r) - \rho N - 1(r) \quad \text{(Electrophilic attack)} \quad [3]$$

$$f^0(r) = \rho N(r) \qquad \text{(Radical attack)}$$

Where, ρN+1, ρN and ρN-1 represent the electron density of anionic, neutral and cationic residues, respectively. Considering the negative charge on sialic acid, we performed Mulliken population analysis to describe the probability of electrostatic interactions (Mulliken, 1955).

$f^+ k = \text{[illegible]}k(N+1) - \text{[illegible]}k(N)$ (Nucleophilic attack) [4]

$f^- k = \text{[illegible]}k(N) - \text{[illegible]}k(N-1)$ (Electrophilic attack) [5]

$f^0 k = \frac{1}{2}(\text{[illegible]}k(N+1) - \text{[illegible]}k(N-1)$ (Radical attack)

Hence, qk (N), qk(N+1) and qk(N-1) are the Mulliken charges at atom k of the neutral, anion and cation species, respectively.

$$f^2(r) = \Delta f(r) \approx \rho N + 1(r) - \rho N - 1(r) - 2\rho N(r) \qquad [6]$$
$$= f^+(r) - f^-(r)$$

The $\Delta \boldsymbol{f}$(r) provides the stabilizing and destabilizing interaction between a nucleophile and an electrophile and helps in distinguishing the nucleophilic/electrophilic nature of a specific site within molecule (Roy et. al., 2005). Donor-acceptor interaction during complex formation was estimated by second order perturbation theory (Andersson, Malmqvist Roos, Sadlej, & Wolinski, 1990). The donor-acceptor interaction represents the charge transfer between acceptor and donor molecules without forming a bond between them. For each donor (*i*) and acceptor (*j*) natural bond orbital (NBO), the standardization energy (E) associated with electron shift was calculated as per Equation [7]:

$$E = -q_{i} \frac{(fij)}{\varepsilon j - \varepsilon i} \qquad [7]$$

where, qi is the donor orbital occupancy, εi and εj are diagonal elements (orbital energies) and F (i, j) is the off-diagonal NBO Fock matrix element.

Hyper-polarizability has been also calculated to reveal the isosurfaces and individual contribution of the molecule. Electronic properties of the highest occupied molecular orbital (HOMO), lowest unoccupied molecular orbital (LUMO) and energy gap (ΔE) were also

determined. HOMO and LUMO dictate the manner in which two molecules interact with each other. To explain reactivity Global hardness (η), global softness (σ), chemical potential (μ), nucleophilicity (N), electrophilicity (ω) and electro negativity (χ) of the molecule were calculated as follows:

$$\eta = \frac{1}{2}(\in_{LUMO} - \epsilon_{HOMO}) \qquad [8]$$

$$\sigma = \frac{1}{2}\eta \qquad [9]$$

$$\mu = -\chi = \frac{1}{2}(\in_{HOMO} + \in_{LUMO}) \qquad [10]$$

$$\omega = \frac{\mu^2}{2\eta} \qquad [11]$$

In addition to electrostatic forces, hydrogen bonding also plays a crucial role in maintaining the complex stability. We analyzed the effect of hydrogen bonding upon ligand–SA interaction by providing vibrational assignments to the interacting groups using DFT. Our calculations are performed with varying pH to know the correct pH environment for the chemotherapy. The inclusion of pH in calculations is done based on the theoretical descriptions provided in 2001, Liptak's report and included in JAGUAR. We briefly describe the formulation, which takes account of pH environment in the DFT calculations.

$$pKa = a\ pKa_{raw} + b \qquad [12]$$

Where, a and b are empirical parameters (Bochevarov et. al., 2016)(Liptal et. al., 2001) and

$$pKa_{raw} = \frac{\Delta G}{2.3RT} \qquad [13]$$

Where, G is the free energy of the deprotonation of the solution, R is Universal gas constant, and T is Temperature. G is approximated by essentially a combination of the gas phase and solution phase DFT energies of the protonated and deprotonated forms of the molecule.

The free energy of the deprotonation of the solution is calculated as:

$$\Delta G = E(A^-)g - E(AH)g - E(AH)solv + E(A^-)solv + Const \qquad [14]$$

Where,

E(A^-)g is the gas phase DFT energy of the protonated form. $E(AH)g$ is gas phase energy of

the protonated form. $E(AH)solv$ is Solvation energy of the protonated form and $E(A^-)solv$ is Solvation energy of the deprotonated form respectively.

Results and Discussion:

Our study models the interaction between extracellular SA residues on cancer cell surface and Gal. Affinity of such ligand-receptor interactions plays a decisive role in cascade initiation which ultimately leads to endocytosis of targeted theranostic carriers (Tiwari et. al., 2017). In addition to numerous physiological factors, interaction energy of ligand-receptor complex depends upon their three dimensional characteristics, such as, stereochemical orientation of neighbouring functional groups and electronic properties. Cumulative strength of this interaction regulates the affinity of ligand-target complex. Keeping in view the biochemical observations, we formulated two hypotheses in this study; ***i***) a diol binding site exists in SA, and ***ii***) the nature of binding remains identical for recognition sugars and sugar-mimetics.

Hypoxia and extracellular acidity are closely associated with tumor progression. Driven by multiple oncogenic factors, tumor tissues produce lactate via anaerobic glycolytic pathway, even in the presence of sufficient oxygen. High lactate, together with other acidic metabolites, corresponds to a high proton concentration, thereby resulting into acidic extracellular pH in solid tumor tissues (Helmlinger, Yuan, Dellian, & Jain, 1997; Kato, Ozawa, Miyamoto, Maehata, Suzuki et. al., 2013). Loco-regional hyperthermia, a local rise in temperature (40−43°C), in synergistic combination with chemotherapy, has gained wide acceptance among surgeons as a tool to melt the tumor mass. It prompts immediate cellular death, probably through hypersensitization of cancer cells toward anti-cancer drugs and has shown improved survival rate among the patients (Hildebrandt, Wust, Ahlers, Dieing, Sreenivasa et. al., 2002; Mauro, Scialabba, Cavallaro, Licciardi, & Giammona, 2015). Motivated by these experimental findings, we modeled the influence of pH alterations and local rise in temperature upon Gal-SA binding. In our simulations, changes in temperature

and pH are expected to influence the vibrational behavior of molecules, thereby altering their binding dynamics and complex stability.

The study was initiated with a simple bimolecular Gal–SA complex. Reactivity descriptors, such as, HOMO (electron donor), LUMO (electron acceptor), HOMO-LUMO gap (HLG), chemical potential (μ), absolute hardness (η), and softness (σ) were calculated using DFT.

Table 1: Summary of calculated reactivity descriptors, HOMO, LUMO, energy gap, hardness, softness and chemical potential, of Gal-SA complex under different temperature and pH conditions.

pH	Temperature (°C)	HOMO (eV)	LUMO (eV)	HLG (eV)	Hardness (η) (eV)	Softness (σ) (eV)	Chemical Potential (μ) (eV)	Electrophilicity (ω) (eV)
5.0	37	-0.24060	-0.00975	0.23085	0.115425	4.232804	-0.125175	-0.06787
	42	-0.23824	-0.01139	0.22685	0.113425	4.408199	-0.124815	-0.06867
5.5	37	-0.24076	-0.01044	0.23032	0.11516	4.341785	-0.1256	-0.06849
	42	-0.24078	-0.00818	0.23260	0.1163	4.299226	-0.12448	-0.06661
6.0	37	-0.23584	-0.01229	0.22355	0.111775	4.473272	-0.124065	-0.06885
	42	-0.23484	-0.01187	0.22297	0.111485	4.484908	-0.123355	-0.06824
6.5	37	-0.24057	-0.01063	0.22994	0.11497	4.348961	-0.1256	-0.06860
	42	-0.24084	-0.01070	0.23014	0.11507	4.345181	-0.12577	-0.06873
7.0	37	-0.23763	-0.00813	0.22950	0.11475	4.357298	-0.12288	-0.06579
	42	-0.23614	-0.01023	0.22591	0.112955	4.426542	-0.123185	-0.06717

Table 1 shows the energy of HOMO and LUMO is directly related to the ionization potential and electron affinity, respectively (Zhan, Nichols, & Dixon, 2003). Smaller energy gap between HOMO–LUMO is conducive to higher charge transfer ability inside the receptor pocket and is associated with higher interaction potential. Conversely, large HOMO–LUMO gap makes the molecule relatively less reactive (Zhan et. al., 2003). A lower HLG value is evident at low pH and hyperthermic condition which is suggestive of greater affinity between Gal and SA at tumor-relevant pH. Orientation of Gal molecule in the vicinity of SA binding pocket resulted into an intra-molecular interaction at π^* C_{22} - O_{23} molecular orbital. This is suggestive of induction of delocalization effect upon SA, a pre-requisite conformational change conducive to binding (Sebastian & Sundaraganesan, 2010).

Binding energy calculations verified the above observations. Binding energy, with and without BSSE, is calculated. However, we report and discuss binding energy only with

BSSE correction (Table 2).

Table 2: Binding energy and distance between two optimized molecules after BSSE correction.

pH	Temperature (˚C)	BSSE (kcal/mol)	$E_{binding}$ (kcal/mol)	Distance (Å)
5.0	37	11.95	-14.55	1.75
	42	9.24	-26.22	1.77
5.5	37	11.91	-14.58	1.78
	42	7.37	-19.94	1.73
6.0	37	11.92	-14.55	2.03
	42	8.06	-26.52	1.67
6.5	37	7.35	-17.41	1.80
	42	7.37	-19.92	1.76
7.0	37	11.21	-19.24	1.73
	42	9.77	-15.79	2.21

Above data shows that an increase in the binding affinity was noticed at 42°C relative to normal physiological temperature. In addition, approximately two-fold improvement in binding (-26.52 kcal/mol in contrast to -14.55 kcal/mol at 37°C) was observed at pH 6.0, a condition typical to the tumour environment. This effect appears to be much stronger possibly than that could be observed experimentally. The effect of temperature upon binding affinity started diminishing with increase in pH. For instance, at normal physiological pH (7.0), the difference between binding energy remained less than 4 kcal. Overall, our measurements revealed that; (*i*) increasing temperature and decreasing pH, in general, have a favourable effect on binding affinity, and (*ii*) induction of hyperthermia at tumour-relevant pH offers pronounced enhancement in the binding affinity. These results point towards a clear relationship between binding affinity and reduced microenvironment pH and elevated temperature. Our calculations are well-supported by experimental findings. Acidic pH responsive drug formulations have shown improved targeting ability and efficacy in animal

models (Min, Kim, Bae, Shin, Kim et. al., 2010; Wu, Kim, Koo, Bae, Shin et. al., 2010). Reduction in binding energy and bond distance did not appear to be proportional (Table 2). This indicates that repulsive forces were operative in some cases which would have resulted into lower binding energy even with lower bond distance.

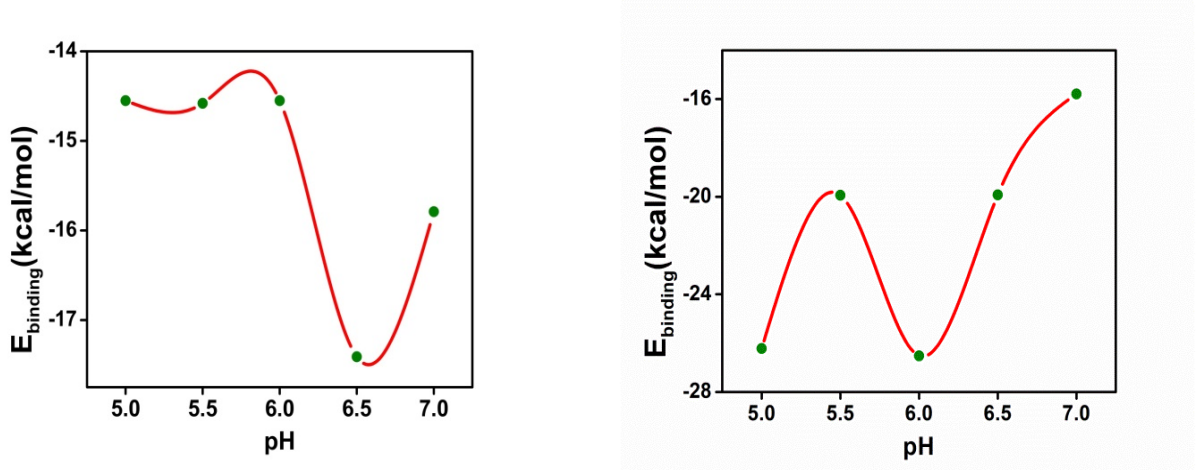

Figure 1: Binding energy curve of SA-Gal complex at 37˚C (a) and 42˚C (b) under various pH conditions.

Bond length in our calculations ranged from 1.67 to 2.21 Å in Figure 1 and Table 2; which points to the involvement of hydrogen bonds (Yourdkhani et. al., 2017). The highest bond length was observed at pH 7.0 and 42˚C. This pH condition is, however, is unrealistic for a solid tumor microenvironment.

In our study, binding energy descriptors were elaborated with a presumption that non-covalent interactions, such as hydrogen bonding and a combination of electrostatic, hydrophobic and van der Waals' interactions, are the predominant contributors. These interactions are, however, weaker (binding constants 10^3–10^4 M^{-1}) in comparison to bio-recognition events. In biological experiments, cooperative polyvalent interactions, achieved

through clustering of binding sites, have shown multi-fold enhancement in the binding affinity (David et. al., 2002; Wu, Li, Chen, Fossey, James et. al., 2013). Therefore, we have modelled the additive effect of ligands' bi-valency over its affinity interaction with SA residues (Table 3). Further, Gal-SA binding energy was compared with that of Man-SA and PBA-SA (Figure 2).

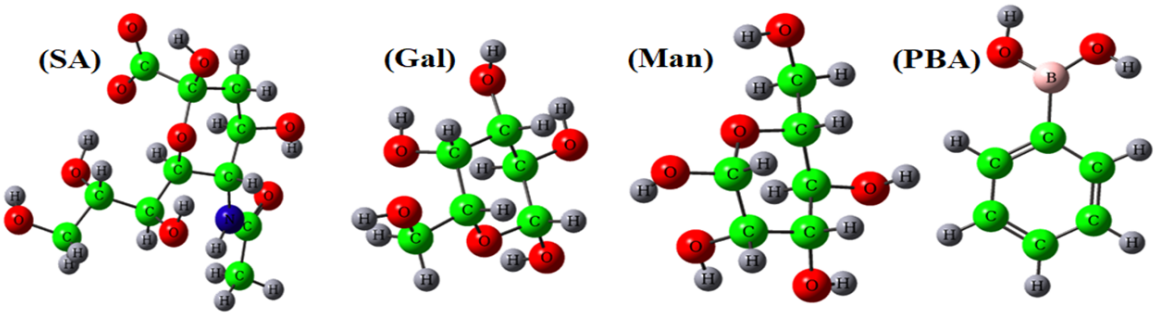

Figure 2: Chemical structure of SA, Monovalent Gal, Man and PBA.

Relative to Man and PBA, Gal exhibited the highest binding affinity (-31.7353) in monovalent configuration (Table 3). Its bivalent construct, however, showed repulsive interaction with SA, an observation which contradicts the experimental reports (David et. al., 2002).

Table 3: Binding energy of ligands under mono- and bi-valent configurations.

Interaction complex	**Configuration of ligand**	**$E_{binding}$(kcal /mol)**	**HOMO**	**LUMO**	**HLG**
Gal-SA	Monovalent	-31.7353	-0.1242	-0.0953	0.0289
	Bivalent	49.8781	-0.1926	-0.0366	0.1559
Man-SA	Monovalent	-23.8794	-0.1235	-0.0667	0.0568
	Bivalent	-54.9871	-0.0396	-0.1529	0.1926
PBA-SA	Monovalent	164.4198	-0.1083	-0.0572	0.0511
	Bivalent	-244.9476	-0.22545	-0.02079	0.20466

A similar contradiction was seen with monovalent PBA-SA interaction. Such observations have been reported in certain experiments as well. For instance, Chen's group studied the effect of number of Man units per nanocarriers (NC) and the distance between mannose units

upon NC uptake in macrophage cells. A decline in the uptake was observed beyond two Man units per NC. Clustering of membrane receptors in association with higher Man units impeded their engagement with NC. Occupancy of ligands receptor binding domain as a function of their inter-atomic and spacer distances can also affect the orientation of ligand under appropriate entropic configuration (Chen, Zhang, Jia, Prud'homme, Szekely et. al., 2014).

Electrostatic interactions originate from the equal sharing of charge density between two participating atoms. These interactions play a crucial role in determining hydrogen bonds between carbohydrate residues, especially for electronically charged molecules (Choi, Kim, Cho, Paik, Kim et. al., 2009; Lienke, Klatt, Robinson, Koch, & Naidoo, 2001). Taking into account the negative charge on SA and a probability of charge-based interaction, we have applied Mulliken charge sets to obtain a point charge between SA and saccharide molecules. Differential charge density within Gal-SA complex was investigated in terms of Mulliken charegcharge (Figure 3).

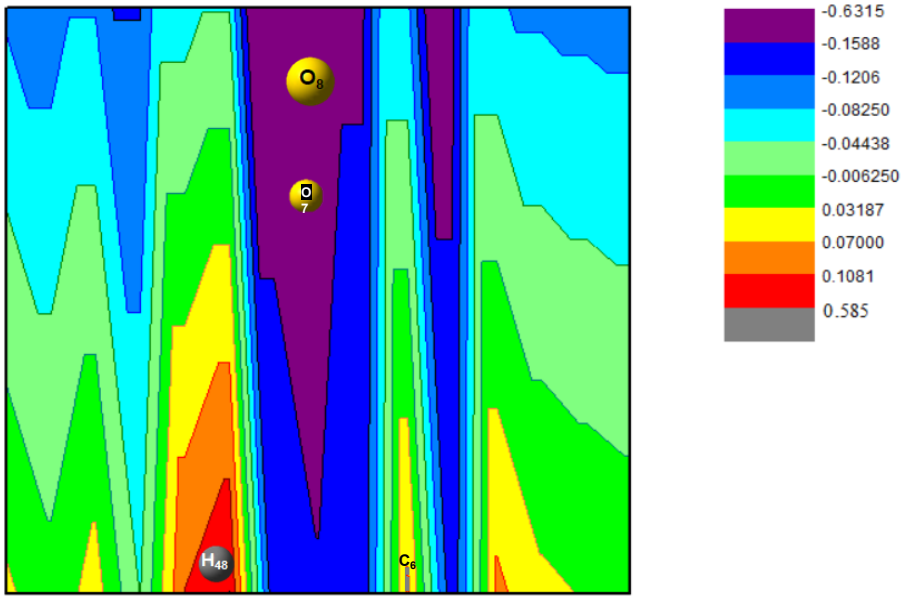

Figure 3: Mulliken charge distribution of SA-Gal complex.

Above figure clearly depicts the atoms involved in the interaction. In addition to reactivity areas, nucleophilic and electrophilic nature of each atom is indicated. Purple colour denotes atoms with comparatively greater negative charge whereas red and grey regions show

positive charge. Atoms O_7 and O_8 in SA, possessing the highest negative charge, appear to be nucleophile acceptors. Atom O_8, carrying a charge of -0.6315, is shown interacting with H_{62} of Gal (+0.3716) with a resultant bond distance of 1.67 Å (Figure 4). A carboxylic acid at the C_6 position and various α-glycosidic linkages to the sugar chain stemmed from O_8 atom.

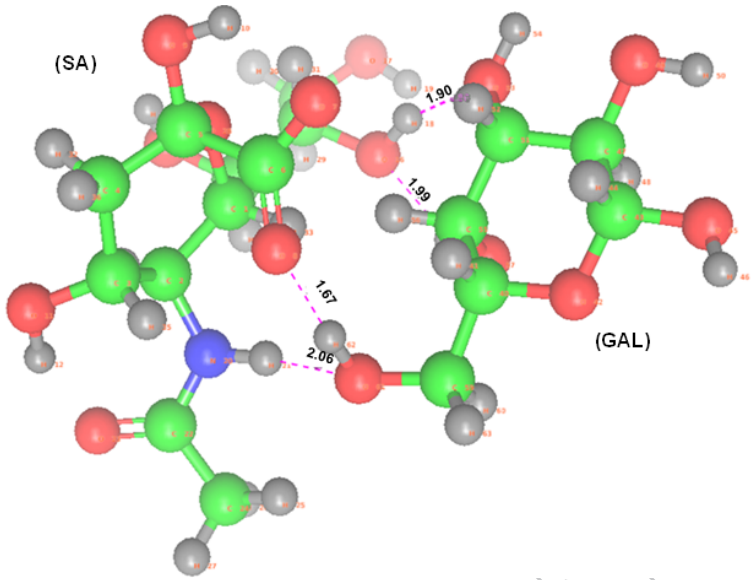

Figure 4: Optimized structure of SA-Gal with the least bond distance (d =1.67Å) between O8-H62.

Considering Gal-SA complex a typical donor-acceptor system, Fukui function f(r) was calculated to probe their reactivity. Charge difference between electrophilic and nucleophilic atoms is indicative of system softness and highlights the active site of the molecule. Improvement in local softness promotes highly affinity interaction at atomic level. In our calculations, C_6, O_8, and O_{28} acted as primary nucleophilic whereas C_{22}, N_{20}, and O_{23} were primary electrophilic attack sites. Besides, O_{23}=C_{22}-N_{20} (nucleophilic) group represented electrophilic attack region for Gal molecule (Table 4).

Table 4: Electrophilicity and nucleophilicity of participating atoms in Gal-SA complex.

Atoms	**f^+**	**f^-**	**f(r)**
C_6	0.0005	0.0636	-0.0631
O_8	0.0001	0.4842	-0.4841
N_{20}	0.1162	0.0002	0.1160
C_{22}	0.4890	-0.0000	0.4890
O_{23}	0.2015	0.0007	0.2008

O_{28}	0.0009	0.0920	-0.0911

NBO calculations pointed towards second order interaction between the highly occupied orbital of one molecule and unoccupied orbital of the other interacting molecules. Charge distribution in the NBO basis set was evaluated by second order Fock matrix. Interaction results showed loss and regain the occupancy in Lewis and non-Lewis orbitals. Equilibrium energy (E^2) was related with the stabilized strength of the two orbitals; electron donor as *i* and acceptor as *j*. Greater tendency of delivering electrons to *j* indicate high affinity interaction. Anti-bonding acceptor orbitals appeared interacting with the lone pair (LP) of O_7, O_8, O_9 and O_{23} (Table S1). Valance electronic configurations of O_7, O_8 and O_9 atoms are $^2s^2p$ (5.00), $^2s^2p$ (5.08) and $^2s^2p$ (5.09), respectively. This indicates the involvement of one unpaired electron and the role of sp hybridization. Highest hyper-conjugative interaction energy (E^2) was shown by LP(3)O_8; σ^*C_6-O_7 (97.72 kcal/mol) and LP(1)N_{20}; π^*C_{22}-O_{23} (51.89 kcal/mol). Other orbitals with higher hyper-conjugative interactions are LP(2)O_7; π^*C_6-O_8, LP(2)O_{23}; σ^*C_{22}-O_{24}, and LP(2)O_9; σ^*C_5-O_{28}.

Theoretical intensities show isolated molecule bending in solid state. The appearance of the hydrogen bonding is much weaker than the van der Waals contact. Table S2 shows the hydrogen bonding between molecules and particular atoms. The fundamental modes of compound for which comprehensive descriptions are discussed below are assigned based on vibrational theory.

The vibrations are influenced by C-C bonds. These vibrations are within the region 1000 to 1300 cm^{-1} (Gunasekaran, Kumaresan, Arunbalaji, Anand, & Srinivasan, 2008), based on experiments. In the present study, the vibrations in SA were observed at 1068 and 1118 cm^{-1} with antisymmetric (C_{24}-C_{22}) and (C_5-C_6) respectively in Raman bands. The galactose has been identified at 1124 cm^{-1} with antisymmetric (C_{40}-C_{59}) and 1416 cm^{-1} with rocking (C_{40}-C_{59}) vibrations. These results show that the theoretical values are better conformity with experimental data. The N-H stretches of amine group is found in 3000 to 3500 cm^{-1} region

(Gunasekaran et. al, 2008). These have been recorded as highest 649 cm^{-1} IR intensity at 3482 cm^{-1} with antisymmeytric (H_{21}-N_{20}) and 3352 cm^{-1} with rocking (H_{21}-N_{20}) vibrations. The O-C stretching Vibrations in structure and its derivatives are in the region 1000 to 1300 cm^{-1}. In this study, Corresponded peaks to O-C vibrations observed at 747 and 1352 cm^{-1} (O_{16}-C_{14}) in SA and 1118 cm^{-1} with antisymmetric (C_{59}-O_{61}) in galactose. IR intensities of structure are 51, 100, and 106 respectively. H-C-C bending is identified in the region 747 to 1434 cm^{-1}. In this study, 6 HCC vibrations of whole complex observed and spotted FT-IR spectra peaks are 33, 36, 79, 103, 106, and 119 cm^{-1}. H-C-H bending is observed in region 1042 to 1068 cm^{-1}. In present study two HCH bending vibrations observed and FT-IR spectra peaks spotted at 53 and 57 cm^{-1}. C-C-C bending is observed in region 229 to 552 cm^{-1}. In this study two CCC vibrations were identified at 10 and 106 cm^{-1} FT-IR peaks. In the present study 11 H-C-N vibrations are spotted in region 747 to 1597 cm^{-1}. Identified FT-IR peaks are at 22, 30, 39, 52, 68, 76, 103, 106, 119, and 258. NCC, OCC, COH, HOO, HCC and OCH are the other bending vibrations that are seen in structure. The occurrences of these vibrations are around ten.

Next, we studied molecular electrostatic potential (MEP), another non-specific interaction parameter, to demonstrate the electron density at Gal-SA complex isosurface (Figure 5).

Figure 5: Molecular electrostatic potential (MEP) at different pH and temperature: (a) pH 5.0; 37˚C, (b) pH 5.0; 42˚C, (c) pH 5.5; 37˚C, (d) pH 5.5; 42˚C, (e) pH 6.0; 37˚C, (f) pH 6.0; 42˚C, (g) pH 6.5; 37˚C, (h) pH 6.5; 37˚C, (i) pH 7.0; 37˚C, and (j) pH 7.0; 42˚C.

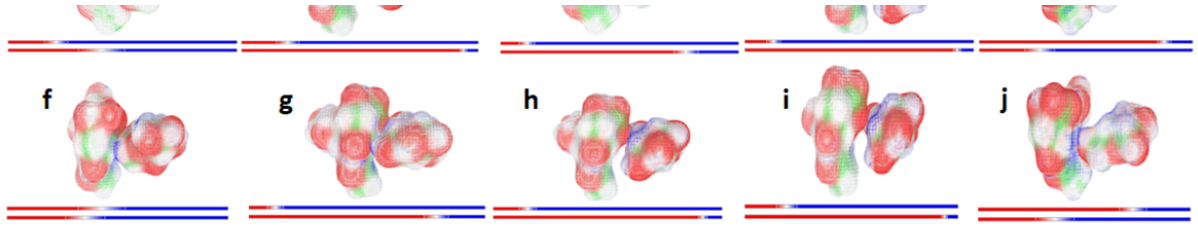

Fig. 5 shows the electrostatic potential map with negative (red) and positive (blue) regions represent nucleophilic and electrophilic reactivity, respectively. Greater electron density is expected within the active sites of SA. Specifically, highest negative and positive electrostatic

potential appeared localized over the oxygen (O_8) and carbon (C_{22}) atoms, respectively. Role microenvironment pH upon creating electron density around nuclei and facilitating Gal-SA interaction is apparent in Fig. 5. The following order of reactivity was observed; f>e>j>b>i>g>h>c>a>d. The highest reactivity for f indicates instability of the complex under high acidic and basic condition. These results, put together with the calculated values of binding energy in Table 2, lead us to conclude that Gal-SA interaction is relatively stronger at tumor-relevant pH (6.0) and under hyperthermic (42˚C) condition. Our observations support the application of pH responsive drug delivery vehicles and targeted hyperthermic chemotherapy for eradicating solid tumor deposits.

Overall, we have adopted a simplistic approach to describe the interaction of a small molecule ligand with extracellular SA. Real targeted theranostic carrier systems are far more complex. Often, they are composed of macromolecular backbones appended with ligand units, often employing spacer molecules and with different degrees of substitution. Therefore, inclusion of carrier-related variables can make the model more realistic. For instance, we have not modeled the possibility of appending Gal over a polymer template, steric influence of pendant groups on Gal-SA interaction and the probability of pre-mature dissociation of Gal from the template under cancer-related physiological insults. In future, this approach will be updated to model a more realistic system through the application of a wider simulation box.

Conclusion:

In this study, we have predicted the affinity of Gal with cell surface SA residues, which are over-expressed in a variety of cancers. Binding energy of molecular orbitals was calculated using gradient-corrected density function theory. Effect of physiological variables, such as pH and temperature, upon the complex stability was also studied. Our calculations demonstrated a stronger Gal-SA interaction at tumor-relevant low pH and hyperthermic condition and therefore, support the application of pH responsive delivery vehicles and

targeted hyperthermic chemotherapy for eradicating solid tumor deposits. These results can be taken as a supportive evidence of the interaction between SA and saccharide ligands at the cancer cell surface. With its wider exploration with other molecular targets, it is speculated that the method can be used as a predictive tool while designing the targeted theranostics for cancer cells.

Conflict of interest: Authors report no conflict of interest.

Acknowledgements: The study was supported by a research grant ECR/2017/000903 and SB/S2/CMP-005/2013 from the Science & Engineering Research Board (SERB), India. Parts of the calculations were performed on SAYAJI Clusters developed under DST-FIST program.

References

Andersson, K., Malmqvist, P. A., Roos, B. O., Sadlej, A. J., & Wolinski, K. (1990) Second-order perturbation theory with a CASSCF reference function. *The Journal of Physical Chemistry, 94*(14), 5483-5488. DOI: 10.1021/j100377a012.

Azab, A. K., Kleinstern, J., Srebnik, M., & Rubinstein, A. (2008) The metastatic stage-dependent mucosal expression of sialic acid is a potential marker for targeting colon cancer with cationic polymers. *Pharmaceutical Research, 25*(2), 379-386. DOI:10.1007/s11095-007-9330-4.

Bloch, M., Kam, Y., Yavin, E., Moradov, D., Nissan, A., Ariel, I., & Rubinstein, A. (2012) The relative roles of charge and a recognition peptide in luminal targeting of colorectal cancer by fluorescent polyacrylamide. *European Journal of Pharmaceutical Sciences, 47*(5), 904-913. DOI:10.1016/j.ejps.2012.09.003.

Bloch, M. B. D., Yavin, E., Nissan, A., Ariel, I., Kenett, R., Brass, D., & Rubinstein, A. (2017) The effect of linker type and recognition peptide conjugation chemistry on tissue affinity and cytotoxicity of charged polyacrylamide. *Journal of Controlled Release, 257*, 102-117. DOI:10.1016/j.jconrel.2016.06.038.

Bochevarov, A. D., Watson, M. A., Greenwood, J. R., & Philipp, D. M. (2016) Multiconformation, Density Functional Theory-Based pKa Prediction in Application to Large, Flexible Organic Molecules with Diverse Functional Groups. *Journal of Chemical Theory and Computation, 12*(12), 6001-6019. DOI:10.1021/acs.jctc.6b00805.

Boys, S. F., & Bernardi, F. D. (1970) The calculation of small molecular interactions by the differences of separate total energies. Some procedures with reduced errors. *Molecular Physics, 19*(4), 553-566. DOI:10.1080/00268977000101561.

Chen, P. M., Zhang, X. P., Jia, L., Prud'homme, R. K., Szekely, Z., & Sinko, P. J. (2014) Optimal structural design of mannosylated nanocarriers for macrophage targeting. *Journal of Controlled Release, 194*, 341-349. DOI: 10.1016/j.jconrel.2014.09.006.

Choi, Y., Kim, H., Cho, K. W., Paik, S. R., Kim, H. W., Jeong, K., & Jung, S. (2009) Systematic probing of an atomic charge set of sialic acid disaccharides for the rational molecular modeling of avian influenza virus based on molecular dynamics simulations. *Carbohydrate Research, 344*(4), 541-544. DOI: 10.1016/j.carres.2008.12.018.

Christian Bharathi, A., Srinivas, S., & Syed Ibrahim, B. (2018) Exploring the binding mechanism and kinetics of Piperine with snake venom secretory Phospholipase A2. *Journal of Biomolecular Structure and Dynamics, 36*(1), 209-220. DOI: 10.1080/07391102.2016.1271750.

David, A., Kopeckova, P., Kopecek. J., & Rubinstein, A. (2002) The role of galactose, lactose, and galactose valency in the biorecognition of N-(2-hydroxypropyl)methacrylamide copolymers by human colon adenocarcinoma cells. *Pharmaceutical Research, 19*(8), 1114-1122. DOI:10.1023/A:1019885807067.

Deshayes, S., Cabral, H., Ishii, T., Miura, Y., Kobayashi, S., Yamashita, T., & Kataoka, K. (2013) Phenylboronic acid-installed polymeric micelles for targeting sialylated epitopes in solid tumors. *Journal of the American Chemical Society, 135*(41), 15501-15507. DOI:10.1021/ja406406h.

Frisch, M. J., Trucks, G. W., Schlegel, H. B., Scuseria, G. E., Robb, M. A., Cheeseman, J. R., … Fox, D. J. (2016) Gaussian, Inc., Wallingford CT.

Fukuda, M. (1996) Possible roles of tumor-associated carbohydrate antigens. *Cancer Research, 56*(10), 2237-2244.

Gunasekaran, S., Kumaresan, S., Arunbalaji, R., Anand G., & Srinivasan, S. (2008) Density functional theory study of vibrational spectra and assignment of fundamental modes of dacarbazine, *Journal of Chemical Sciences***,** *120*(3), 315-324. DOI: 10.1007/s12039-008-0054-8.

Guo, H. B., Nairn, A., Harris, K., Randolph, M., Alvarez-Manilla, G., Moremen, K., & Pierce, M. (2008) Loss of expression of N-acetylglucosaminyltransferase Va results in altered gene expression of glycosyltransferases and galectins. *FEBS Letters.*, 582(4), 527-535. DOI:10.1016/j.febslet.2008.01.015.

Hakomori, S. (2002) Glycosylation defining cancer malignancy: new wine in an old bottle. *Proceedings of the National Academy of Sciences of the United States of America*, *99*(16), 10231-10233 DOI:10.1073/pnas.172380699.

Helmlinger, G., Yuan, F., Dellian, M., & Jain, R. K. (1997) Interstitial pH and pO2 gradients in solid tumors in vivo: high-resolution measurements reveal a lack of correlation. *Nature Medicine, 3*(2), 177-182. DOI: 10.1038/nm0297-177.

Hildebrandt, B., Wust, P., Ahlers, O., Dieing, A., Sreenivasa, G., Kerner, T., Felix., & Riess, H. (2002) The cellular and molecular basis of hyperthermia. *Critical Reviews in Oncology/Hematology, 43*(1), 33-56. DOI: 10.1016/S1040-8428(01)00179-2.

Kato, Y., Ozawa, S., Miyamoto, C., Maehata, Y., Suzuki, A., Maeda, T., & Baba, Y. (2013)

Acidic extracellular microenvironment and cancer. *Cancer Cell International, 13*(1), 89-96. DOI:10.1186/1475-2867-13-89.

Kim, Y. J., & Varki, A. (1997) Perspectives on the significance of altered glycosylation of glycoproteins in cancer. *Glycoconjugate Journal, 14*(5), 569-576. DOI:10.1023/A:1018580324971

Kohnz, R. A., Roberts, L. S., DeTomaso, D., Bideyan, L., Yan, P., Bandyopadhyay, S., & Nomura, D. K. (2016) Protein sialylation regulates a gene expression signature that promotes breast cancer cell pathogenicity. *ACS Chemical Biology, 11*(8), 2131-2139. DOI:10.1021/acschembio.6b00433.

Lee, C., Yang, W., & Parr, R. G. (1988) Development of the Colle-Salvetti correlation-energy formula into a functional of the electron density. *Physical Review B, 37*(2), 785-789. DOI:10.1103/PhysRevB.37.785.

Lee, J. Y., Chung, S. J., Cho, H. J., & Kim, D. D. (2015) Phenylboronic acid-decorated chondroitin sulfate a-based theranostic nanoparticles for enhanced tumor targeting and penetration. *Advanced Functional Materials, 25*(24), 3705-3717. DOI: 10.1002/adfm.201500680.

Lienke, A., Klatt, G., Robinson, D. J., Koch, K. R., & Naidoo, K. J. (2001) Modeling platinum group metal complexes in aqueous solution. *Inorganic Chemistry, 40*(10), 2352-2357. DOI: 10.1021/ic0005745.

Liptak, M.D., & Shields, G.C. (2001). Accurate pKa calculations for carboxylic acids using complete basis set and Gaussian-n models combined with CPCM continuum solvation methods. *Journal of the American Chemical Society, 123*(30), 7314-7319. DOI: 10.1021/ja010534f.

Manoharan, P., Chennoju, K., & Ghoshal, N. (2018) Computational analysis of BACE1-ligand complex crystal structures and linear discriminant analysis for identification of BACE1 inhibitors with anti P-glycoprotein binding property. *Journal of Biomolecular*

Structure and Dynamics, 36(1), 262-276. DOI: 10.1080/07391102.2016.1276477.

Mauro, N., Scialabba, C., Cavallaro, G., Licciardi, M., & Giammona, G. (2015) Biotin-containing reduced graphene oxide-based nanosystem as a multieffect anticancer agent: combining hyperthermia with targeted chemotherapy. *Biomacromolecules, 16*(9), 2766-2775. DOI: 10.1021/acs.biomac.5b00705.

Min, K. H., Kim, J. H., Bae, S. M., Shin, H., Kim, M. S., Park, S., Lee H., Park, R. W., Kim, I. S., Kim, K., & Known, I. C. (2010) Tumoral acidic pH-responsive MPEG-poly(beta-amino ester) polymeric micelles for cancer targeting therapy. *Journal of Controlled Release, 144*(2), 259-266. DOI: 10.1016/j.jconrel.2010.02.024.

Mohammadi, T., & Ghayeb, Y., (2018) Atomic insight into designed carbamate-based derivatives as acetylcholine esterase (AChE) inhibitors: a computational study by multiple molecular docking and molecular dynamics simulation. *Journal of Biomolecular Structure and Dynamics, 36*(1), 126-138. DOI: 10.1080/07391102.2016.1268977.

MS Jaguar, Schrödinger, LLC, New York, NY, 2017.

Mulliken, R. S. (1955) Electronic population analysis on LCAO-MO molecular wave functions. *Journal of Chemical Physics, 23*(10), 1833-1840. DOI: 10.1063/1.1740588.

Pardhi, T., & Vasu, K. (2018) Identification of dual kinase inhibitors of CK2 and GSK3β: combined qualitative and quantitative pharmacophore modeling approach. *Journal of Biomolecular Structure and Dynamics, 36*(1), 177-194. DOI: 10.1080/07391102.2016.1270856.

Pitchumani Violet Mary, C., Shankar, R., & Vijayakumar, S.; (2018) Theoretical studies on the interaction between the nitrile-based inhibitors and the catalytic triad of Cathepsin K. *Journal of Biomolecular Structure and Dynamics, 36*(3), 634-655. DOI: 10.1080/07391102.2017.1289863.

Prabhu, D., Rajamanikandan, S., Amala, M., Kanagarajan, S., & Jeyakanthan, J. (2018) Identification of Anti-filarial leads against Aspartate semialdehyde Dehydrogenase of

Wolbachia endosymbiont of Brugia malayi: Combined Molecular Docking and Molecular Dynamics Approaches. *Journal of Biomolecular Structure and Dynamics*, (just-accepted) 1-38. DOI:10.1080/07391102.2018.1427633.

Quesne, M.G. Ward, R.A., & de Visser, S.P. (2013). Cysteine protease inhibition by nitrile-based inhibitors: a computational study. *Frontiers in chemistry, 1*(39), 1-10. DOI:10.3389/fchem.2013.00039.

Redondo, P. D. A. G., Nakamura, C. V., De Souza, W., & Morgado-Diaz, J. A. (2004) Differential expression of sialic acid and N-acetylgalactosamine residues on the cell surface of intestinal epithelial cells according to normal or metastatic potential. *Journal of Histochemistry & Cytochemistry, 52*(5), 629-640. DOI:10.1177/002215540405200507.

Regueiro-Figueroa, M., Djanashvili, K., Esteban-Gómez, D., de Blas, A., Platas-Iglesias, C., & Rodríguez-Blas, T. (2010). Towards Selective Recognition of Sialic Acid Through Simultaneous Binding to Its cis-Diol and Carboxylate Functions. *European Journal of Organic Chemistry, 17*, 3237-3248. DOI: 10.1002/ejoc.201000186.

Roy, R. K., Usha, V., Paulovic, J., & Hirao, K. (2005) Are the local electrophilicity descriptors reliable indicators of global electrophilicity trends? *Journal of Physical Chemistry A, 109*(20), 4601-4606. DOI: 10.1021/jp046505j.

Sebastian, S., & Sundaraganesan, N., (2010) The spectroscopic (FT-IR, FT-IR gas phase, FT-Raman and UV) and NBO analysis of 4-Hydroxypiperidine by density functional method. Spectrochimica Acta Part A, Spectrochimica Acta Part A: *Molecular and Biomolecular Spectroscopy, 75*(3), 941-952. DOI: 10.1016/j.saa.2009.11.030.

Tanaka, S. I., Goi, T., Tanaka, K., & Fukase, K. (2007). Highly Efficient α-Sialylation by Virtue of Fixed Dipole Effects of N-Phthalyl Group: Application to Continuous Flow Synthesis of α (2-3)-and α (2-6)-Neu5Ac-Gal Motifs by Microreactor. *Journal of Carbohydrate Chemistry, 26*(7), 369-394. DOI: 10.1080/07328300701634796.

Tiwari, S., Tirosh, B., & Rubinstein, A. (2017) Increasing the affinity of cationized

polyacrylamide-paclitaxel nanoparticles towards colon cancer cells by a surface recognition peptide. *International Journal of Pharmaceutics, 531*(1), 281-291. DOI:10.1016/j.ijpharm.2017.08.092.

Varki, N. M., & Varki, A. (2007) Diversity in cell surface sialic acid presentations: implications for biology and disease. *Laboratory Investigation*, *87*(9), 851-857. DOI:10.1038/labinvest.3700656.

Wang, J., Wu, W., Zhang, Y., Wang, X., Qian, H., Liu, B., & Jiang, X. (2014) The combined effects of size and surface chemistry on the accumulation of boronic acid-rich protein nanoparticles in tumors. *Biomaterials, 35*(2), 866-878. DOI:10.1016/j.biomaterials.2013.10.028.

Wang, S., Wen, Y., Wang, Y., Ma, Y., & Liu, Z. (2017) Pattern Recognition of Cells via Multiplexed Imaging with Monosaccharide-Imprinted Quantum Dots. *Analytical Chemistry, 89*(10), 5646-5652. DOI:10.1021/acs.analchem.7b00965.

Wang, S., Yin, D., Wang, W., Shen, X., Zhu, J. J., Chen, H. Y., & Liu, Z. (2016) Targeting and imaging of cancer cells via monosaccharide-imprinted fluorescent nanoparticles. *Scientific Reports, 6*, 22757-22767. DOI:10.1038/srep22757.

Wu, X. L., Kim, J. H., Koo, H., Bae, S. M., Shin, H., Kim, M. S., Lee, B. H., Park, R W., Kim, I. S., Choi, K., & Known, I. C. (2010) Tumor-targeting peptide conjugated pH-responsive micelles as a potential drug carrier for cancer therapy. *Bioconjugate Chemistry*, 21(2), 208-213. DOI: 10.1021/bc9005283.

Wu, X., Li, Z., Chen, X. X., Fossey, J. S., James, T. D., & Jiang, Y. B. (2013) Selective sensing of saccharides using simple boronic acids and their aggregates. *Chemical Society Reviews, 42*(20), 8032-8048. DOI: 10.1039/C3CS60148J.

Zhan, C. G., Nichols, J. A., & Dixon, D.A. (2003) Ionization potential, electron affinity, electronegativity, hardness, and electron excitation energy: molecular properties from density functional theory orbital energies. *Journal of Physical Chemistry A, 107*(20), 4184–4195.

DOI: 10.1021/jp0225774.

Supplementary information for

Theoretical Investigations and density functional theory based probe of the affinity interaction of saccharide ligands with extra-cellular sialic acid residues

Anjali Patel[1], Sanjay Tiwari[2,*] and Prafulla K Jha[1,*]

[1]Department of Physics, Faculty of Science, The Maharaja Sayajirao University of Baroda, Vadodara- 390 002, Gujarat, India

[2]UKA Tarsadia University, Maliba Pharmacy College, Gopal-Vidyanagar Campus, Surat, 394350, Gujarat, India

[*]Email: tiwarisanju@gmail.com, prafullaj@yahoo.com

Table S1: Electron acceptor, donor percentage and bond type of each interacted atom.

Donor(i) (occupancy)	Type	ED_A % ED_B %	Acceptor(j) (occupancy)	Type	ED_A % ED_B %	$E^{(2)a}$ (kcal/mol)	E_j-E_i^b (a.u.)	$F_{(ij)}^c$ (a.u.)
CR (1) C1 1.99902	σ	-	BD* (1)C1-O28 0.02939	σ*	67.26 32.74	0.95	10.42	0.089
CR (1) C1 1.99902	σ	-	BD* (1)C5-O28 0.10041	σ*	69.96 30.04	0.79	10.37	0.081
CR (1) C2 1.99912	σ	-	BD*(1)N20-C22 0.06556	σ*	37.50 62.50	0.77	10.57	0.081
CR (1) C3 1.99908	σ	-	BD* (1) C3-O11 0.02483	σ*	66.47 33.53	1.10	10.42	0.096
CR (1)C5 1.99898	σ	-	BD* (1)C1-O28 0.02939	σ*	67.26 32.74	0.77	10.47	0.080
CR (1)C5 1.99898	σ	-	BD* (1)C4-C5 0.03863	σ*	49.52 50.48	0.67	10.56	0.075
CR (1)C5 1.99898	σ	-	BD* (1)C5-O28 0.10041	σ*	69.96 30.04	0.71	10.42	0.077
CR (1)C5 1.99898	σ	-	BD* (1)O9-H10	σ*	22.85 77.15	0.62	10.61	0.072

			0.05186					
CR (1)O7 1.99978	σ	-	BD* (1)C6-O8 0.05474	π*	66.80 33.20	0.83	19.42	0.113
CR (1)O8 1.99971	σ	-	BD* (1)C6-O7 0.37035	σ*	66.38 33.62	0.88	19.44	0.116
CR C13 1.99902	σ	-	BD*(1)C13-O37 0.02052	σ*	66.83 33.17	1.06	10.41	0.094
CR (1)C14 1.99907	σ	-	BD*(1)C14-O16 0.03030	σ*	68.04 31.96	1.16	10.39	0.098
CR (1)C15 1.99923	σ	-	BD*(1)C15-O17 0.01063	σ*	66.72 33.28	1.03	10.42	0.092
CR (1)N20 1.99934	σ	-	BD*(1)C22-O23 0.04451	π*	65.90 34.10	0.62	14.71	0.086
CR (1)C22 1.99939	σ	-	BD* (1)C2-N20 0.02675	σ*	62.16 37.84	1.24	10.52	0.102
CR (1)C22 1.99939	σ	-	BD*(1)N20-H21 0.03952	σ*	26.41 73.59	0.76	10.65	0.080
CR (1)O23 1.99977	σ	-	BD*(1)N20-C22 0.06556	σ*	37.50 62.50	0.62	19.36	0.098
CR (1)O23 1.99977	σ	-	BD*(1)C22-C24 0.05333	σ*	51.46 48.54	0.67	19.24	0.102
CR (1)C24 1.99937	σ	-	BD*(1)C22-O23 0.04451	π*	65.90 34.10	0.57	10.61	0.069
LP (1)O7 1.97033	σ	-	BD* (1)C5-C6 0.12449	σ*	46.42 53.58	3.11	1.00	0.050
LP (1)O7 1.97033	σ	-	BD* (1)C6-O8 0.05474	π*	66.80 33.20	1.19	1.23	0.034
LP (1)O7 1.97033	σ	-	BD* (1)O9-H10 0.05186	σ*	22.85 77.15	2.62	1.11	0.048
LP (2)O7 1.97033	σ	-	BD* (1)C4-C5 0.03863	σ*	49.52 50.48	0.67	0.63	0.018
LP (2)O7 1.97033	σ	-	BD* (1)C5-C6 0.12449	σ*	46.42 53.58	16.52	0.58	0.087
LP (2)O7 1.97033	σ	-	BD* (1)C6-O8 0.05474	π*	66.80 33.20	22.18	0.81	0.119
LP (2)O7 1.97033	σ	-	BD* (1)O9-H10 0.05186	σ*	22.85 77.15	2.62	1.11	0.048
LP (1) O8 1.93135	σ	-	BD* (1)C3-H35 0.03385	σ*	37.58 62.42	0.56	1.13	0.022
LP (1) O8 1.93135	σ	-	BD* (1)C5-C6 0.12449	σ*	46.42 53.58	0.71	1.00	0.024
LP (1) O8 1.93135	σ	-	BD* (1)C6-O7 0.05312	σ*	66.38 33.62	4.33	1.23	0.065
LP (2)O8	σ	-	BD* (1)C3-	σ*	66.47	0.63	0.56	0.017

1.88814			O11 0.02483		33.53			
LP (2)O8 1.88814	σ	-	BD* (1)C3-H35 0.03385	σ*	37.58 62.42	0.65	0.72	0.019
LP (2)O8 1.88814	σ	-	BD* (1)C5-C6 0.12449	σ*	46.42 53.58	19.30	0.59	0.095
LP (2)O8 1.88814	σ	-	BD* (1)C5-O9 0.03764	σ*	66.92 33.08	0.91	0.60	0.021
LP (2)O8 1.88814	σ	-	BD* (1)C6-O7 0.05312	σ*	66.38 33.62	16.12	0.82	0.102
LP (2)O8 1.88814	σ	-	BD* (2)C6-O7 0.37035	σ*	74.46 25.54	0.60	0.28	0.012
LP (3)O8 1.88814	σ	-	BD* (2)C6-O7 0.37035	σ*	74.46 25.54	97.72	0.27	0.145
LP (1)O9 1.97666	σ	-	BD* (1)C5-C6 0.12449	σ*	46.42 53.58	3.49	0.91	0.050
LP (2)O9 1.905O9	σ	-	BD* (1)C1-O28 0.02939	σ*	67.26 32.74	0.71	0.59	0.018
LP (2)O9 1.905O9	σ	-	BD* (1)C4-C5 0.03863	σ*	49.52 50.48	2.48	0.67	0.036
LP (2)O9 1.905O9	σ	-	BD* (1)C5-C6 0.12449	σ*	46.42 53.58	1.26	0.62	0.025
LP (2)O9 1.905O9	σ	-	BD* (1)C5-O28 0.10041	σ*	69.96 30.04	21.01	0.54	0.095
LP (1)O11 1.97729	σ	-	BD* (1)C2-C3 0.04675	σ*	47.83 52.17	1.89	0.93	0.037
LP (1)O11 1.97729	σ	-	BD* (1)C3-C4 0.02430	σ*	50.57 49.43	1.12	0.96	0.029
LP (1)O11 1.97729	σ	-	BD* (1)C3-H35 0.033385	σ*	37.58 62.42	0.84	1.04	0.026
LP (2)O11 1.95721	σ	-	BD* (1)C2-C3 0.04675	σ*	47.83 52.17	5.20	0.64	0.051
LP (2)O11 1.95721	σ	-	BD* (1)C3-H35 0.033385	σ*	37.58 62.42	7.05	0.75	0.065
LP (1)O16 1.96834	σ	-	BD*(1)C14-H31 0.02469	σ*	37.83 62.17	2.72	1.04	0.048
LP (1)O16 1.96834	σ	-	BD*(1)O17-H19 0.02204	σ*	25.14 74.86	0.68	1.05	0.024
LP (2)O16 1.93743	σ	-	BD*(1)C13-C14 0.04624	σ*	50.22 49.78	4.96	0.69	0.052
LP (2)O16 1.93743	σ	-	BD*(1)C13-O37 0.02052	σ*	66.83 33.17	0.96	0.61	0.022
LP (2)O16 1.93743	σ	-	BD*(1)C14-C15 0.04028	σ*	49.20 50.80	4.99	0.69	0.052

LP (2)O16 1.93743	σ	-	BD*(1)C15-H30 0.01718	σ*	38.28 61.72	0.65	0.79	0.020
LP (2)O16 1.93743	σ	-	BD*(1)O17-H19 0.02204	σ*	25.14 74.86	2.77	0.78	0.041
LP (1)O17 1.98266	σ	-	BD*(1)C14-C15 0.04028	σ*	49.20 50.80	1.70	0.96	0.036
LP (1)O17 1.98266	σ	-	BD*(1)C15-H29 0.03144	σ*	39.81 60.19	0.89	1.02	0.027
LP (1)O17 1.98266	σ	-	BD*(1)C15-H30 0.01718	σ*	38.28 61.72	1.32	1.06	0.033
LP (2)O17 1.95605	σ	-	BD*(1)C13-C14 0.04624	σ*	50.22 49.78	0.72	0.65	0.019
LP (2)O17 1.95605	σ	-	BD*(1)C14-C15 0.04028	σ*	49.20 50.80	4.87	0.65	0.050
LP (2)O17 1.95605	σ	-	BD*(1)C15-H29 0.03144	σ*	39.81 60.19	7.40	0.72	0.065
LP (1)N20 1.67980	σ	-	BD* (1)C1-C2 0.3956	σ*	50.72 49.28	1.00	0.63	0.022
LP (1)N20 1.67980	σ	-	BD* (1)C1-O28 0.02939	σ*	67.26 32.74	0.59	0.58	0.016
LP (1)N20 1.67980	σ	-	BD* (1)C2-C3 0.04675	σ*	47.83 52.17	8.02	0.63	0.063
LP (1)N20 1.67980	σ	-	BD* (1)C2-H34 0.02504	σ*	36.22 63.78	2.01	0.73	0.034
LP (1)N20 1.67980	σ	-	BD* (1)C3-C4 0.02430	σ*	50.57 49.43	0.57	0.66	0.017
LP (1)N20 1.67980	σ	-	BD*(1)N20-H21 0.03952	σ*	26.41 73.59	0.82	0.73	0.022
LP (1)N20 1.67980	σ	-	BD*(1)C22-O23 0.04451	π*	65.90 34.10	4.29	0.78	0.052
LP (1)N20 1.67980	σ	-	BD*(2)C22-O23 0.029952	π*	71.71 28.29	51.89	0.30	0.112
LP (1)O23 1.96859	σ	-	BD*(1)O11-H12 0.03659	σ*	23.58 76.42	3.61	1.17	0.058
LP (1)O23 1.96859	σ	-	BD*(1)N20-C22 0.06556	σ*	37.50 62.50	3.71	1.17	0.059
LP (1)O23 1.96859	σ	-	BD*(1)C22-C24 0.05333	σ*	51.46 48.54	0.97	1.04	0.028
LP (2)O23 1.86818	σ	-	BD*(1)O11-H12	σ*	23.58 76.42	7.50	0.75	0.067

			0.03659					
LP (2)O23 1.86818	σ	-	BD*(1)N20-C22 0.06556	σ*	37.50 62.50	20.38	0.76	0.111
LP (2)O23 1.86818	σ	-	BD*(1)C22-C24 0.05333	σ*	51.46 48.54	21.22	0.63	0.103
LP (1)O28 1.94881	σ	-	BD* (1)C1-C2 0.03956	σ*	50.72 49.28	3.65	0.90	0.051
LP (1)O28 1.94881	σ	-	BD* (1)C1-C13 0.03877	σ*	49.68 50.32	0.94	0.92	0.026
LP (1)O28 1.94881	σ	-	BD* (1)C4-C5 0.03863	σ*	37.58 62.42	1.63	0.94	0.035
LP (1)O28 1.94881	σ	-	BD* (1)C5-O9 0.03764	σ*	66.92 33.08	3.60	0.90	0.051
LP (1)O28 1.94881	σ	-	BD*(1)C13-H39 0.02518	σ*	66.83 33.17	0.52	1.00	0.020
LP (1)O28 1.94881	σ	-	BD*(1)O37-H38 0.02238	σ*	24.44 75.56	1.28	1.00	0.032
LP (2)O28 1.91688	σ	-	BD* (1)C1-C2 0.03956	σ*	49.68 50.32	3.78	0.67	0.045
LP (2)O28 1.91688	σ	-	BD* (1)C1-H33 0.03884	σ*	38.27 61.73	7.59	0.79	0.069
LP (2)O28 1.91688	σ	-	BD* (1)C4-C5 0.03863	σ*	37.58 62.42	2.95	0.71	0.041
LP (2)O28 1.91688	σ	-	BD* (1)C4-H36 0.01235	σ*	37.45 62.55	0.70	0.77	0.021
LP (2)O28 1.91688	σ	-	BD* (1)C5-C6 0.12449	σ*	46.42 53.58	5.37	0.65	0.053
LP (2)O28 1.91688	σ	-	BD* (1)C6-O7 0.05312	σ*	66.38 33.62	1.89	0.34	0.023
LP (2)O28 1.91688	σ	-	BD*(1)O37-H38 0.02238	σ*	24.44 75.56	2.39	0.77	0.038
LP (1)O37 1.98061	σ	-	BD*(1)C1-C13 0.03877	σ*	49.68 50.32	2.39	0.96	0.043
LP (1)O37 1.98061	σ	-	BD*(1)C13-H39 0.02518	σ*	66.83 33.17	1.08	1.05	0.030
LP (2)O37 1.94810	σ	-	BD*(1)C1-C13 0.03877	σ*	49.68 50.32	2.87	0.66	0.039
LP (2)O37 1.94810	σ	-	BD* (1)C2-H34 0.02504	σ*	36.22 63.78	0.63	0.75	0.019
LP (2)O37 1.94810	σ	-	BD*(1)C13-C14 0.04624	σ*	50.22 49.78	7.53	0.66	0.063
LP (2)O37 1.94810	σ	-	BD*(1)C13-H39	σ*	66.83 33.17	1.00	0.74	0.024

			0.02518					
LP (2)O37 1.94810	σ	-	BD*(1)C14-O16 0.03030	σ*	68.04 31.96	1.93	0.57	0.030
BD(1)C1-C2 1.97505	σ	49.28 50.72	BD*(1)C1-C13 0.03877	σ*	49.68 50.32	1.02	0.98	0.028
BD(1)C1-C2 1.97505	σ	49.28 50.72	BD* (1)C1-H33 0.03884	σ*	38.27 61.73	0.72	1.08	0.025
BD(1)C1-C2 1.97505	σ	49.28 50.72	BD* (1)C2-C3 0.04675	σ*	47.83 52.17	0.62	0.96	0.022
BD(1)C1-C2 1.97505	σ	49.28 50.72	BD* (1)C2-H34 0.02504	σ*	36.22 63.78	0.73	1.07	0.025
BD(1)C1-C2 1.97505	σ	49.28 50.72	BD* (1)C3-O11 0.02483	σ*	66.47 33.53	1.45	0.92	0.033
BD(1)C1-C2 1.97505	σ	49.28 50.72	BD*(1)C13-C14 0.04624	σ*	50.22 49.78	1.90	0.98	0.039
BD(1)C1-C2 1.97505	σ	49.28 50.72	BD*(1)N20-C22 0.06556	σ*	37.50 62.50	2.82	1.09	0.049
BD (1)C1-C13 1.97590	σ	50.32 49.68	BD* (1)C1-C2 0.03956	σ*	50.72 49.28	0.80	0.97	0.025
BD (1)C1-C13 1.97590	σ	50.32 49.68	BD* (1)C1-H33 0.03884	σ*	38.27 61.73	1.00	1.09	0.029
BD (1)C1-C13 1.97590	σ	50.32 49.68	BD* (1)C2-C3 0.04675	σ*	47.83 52.17	1.82	0.97	0.037
BD (1)C1-C13 1.97590	σ	50.32 49.68	BD* (1)C5-O28 0.10041	σ*	69.96 30.04	3.03	0.87	0.046
BD (1)C1-C13 1.97590	σ	50.32 49.68	BD*(1)C13-C14 0.04624	σ*	50.22 49.78	0.68	0.99	0.023
BD (1)C1-C13 1.97590	σ	50.32 49.68	BD*(1)C13-H39 0.02518	σ*	37.97 62.03	0.72	1.06	0.025
BD (1)C1-C13 1.97590	σ	50.32 49.68	BD*(1)C14-C15 0.04028	σ*	49.20 50.80	1.51	0.99	0.035
BD (1)C1-O28 1.98563	σ	32.74 67.26	BD* (1)C2-N20 0.02675	σ*	62.16 37.84	0.99	1.15	0.030
BD (1)C1-O28 1.98563	σ	32.74 67.26	BD* (1)C5-O9 0.03764	σ*	66.92 33.08	1.30	1.17	0.035
BD (1)C1-O28 1.98563	σ	32.74 67.26	BD*(1)C13-H39 0.02518	σ*	37.97 62.03	1.22	1.27	0.035
BD (1)C1-H33	σ	61.73 38.27	BD* (1)C2-N20	σ*	62.16 37.84	0.76	0.85	0.023

1.97507			0.02675					
BD (1)C1-H33 1.97507	σ	61.73 28.27	BD* (1)C2-H34 0.02504	σ*	36.22 63.78	0.72	1.05	0.025
BD (1)C1-H33 1.97507	σ	61.73 28.27	BD*(1)C13-O37 0.02052	σ*	66.83 33.17	3.67	0.81	0.049
BD (1)C2-C3 1.97660	σ	52.17 47.83	BD* (1)C1-C2 0.03956	σ*	50.72 49.28	1.08	0.95	0.029
BD (1)C2-C3 1.97660	σ	52.17 47.83	BD* (1)C1-C13 0.03877	σ*	49.68 50.32	1.38	0.97	0.033
BD (1)C2-C3 1.97660	σ	52.17 47.83	BD* (1)C2-H34 0.02504	σ*	36.22 63.78	0.72	1.05	0.025
BD (1)C2-C3 1.97660	σ	52.17 47.83	BD* (1)C3-C4 0.02430	σ*	50.57 49.43	0.75	0.99	0.024
BD (1)C2-C3 1.97660	σ	52.17 47.83	BD* (1)C4-H36 0.01235	σ*	37.45 62.55	1.41	1.05	0.034
BD (1)C2-N20 1.98259	σ	37.84 62.16	BD* (1)C1-O28 0.02939	σ*	67.26 32.74	1.90	1.04	0.040
BD (1)C2-N20 1.98259	σ	37.84 62.16	BD* (1)C3-C4 0.02430	σ*	50.57 49.43	1.06	1.13	0.031
BD (1)C2-N20 1.98259	σ	37.84 62.16	BD*(1)N20-H21 0.03952	σ*	26.41 73.59	0.52	1.20	0.022
BD (1)C2-N20 1.98259	σ	37.84 62.16	BD*(1)N20-C22 0.03952	σ*	37.50 62.50	1.38	1.22	0.037
BD (1)C2-N20 1.98259	σ	37.84 62.16	BD*(1)C22-C24 0.05333	σ*	51.46 48.54	2.63	1.09	0.048
BD (1) C2-H34 1.97204	σ	63.78 36.22	BD* (1)C1-H33 0.03884	σ*	38.27 61.73	1.76	0.98	0.037
BD (1) C2-H34 1.97204	σ	63.78 36.22	BD* (1)C3-O11 0.02483	σ*	66.47 33.53	1.58	0.81	0.032
BD (1) C2-H34 1.97204	σ	63.78 36.22	BD* (1)C3-H35 0.03385	σ*	37.58 62.42	0.70	1.07	0.024
BD (1) C2-H34 1.97204	σ	63.78 36.22	BD*(1)N20-H21 0.03952	σ*	26.41 73.59	2.78	0.96	0.046
BD (1)C3-C41.97615	σ	49.43 50.57	BD* (1)C2-C3 0.04675	σ*	47.83 52.17	0.62	0.95	0.022
BD (1)C3-C41.97615	σ	49.43 50.57	BD* (1)C2-N20 0.02675	σ*	62.16 37.84	1.77	0.93	0.036
BD (1)C3-C41.97615	σ	49.43 50.57	BD* (1)C3-H35 0.03385	σ*	37.58 62.42	0.70	1.07	0.024

BD (1)C3-C41.97615	σ	49.43 50.57	BD* (1)C4-C5 0.03863	σ*	49.52 50.48	0.79	0.99	0.025
BD (1)C3-C41.97615	σ	49.43 50.57	BD* (1)C4-H32 0.01562	σ*	37.46 62.54	0.68	1.05	0.024
BD (1)C3-C41.97615	σ	49.43 50.57	BD* (1)C4-H36 0.01235	σ*	37.45 62.55	0.065	1.05	0.023
BD (1)C3-C41.97615	σ	49.43 50.57	BD* (1)C5-O9 0.03764	σ*	66.92 33.08	2.50	0.95	0.044
BD (1)C3-C4 1.97615	σ	49.43 50.57	BD*(1)O11-H12 0.03659	σ*	23.58 76.42	1.57	1.07	0.037
BD (1)C3-O11 1.99204	σ	33.53 66.47	BD* (1)C1-C2 0.03956	σ*	50.72 49.28	1.24	1.15	0.034
BD (1)C3-O11 1.99204	σ	33.53 66.47	BD* (1)C4-C5 0.03638	σ*	49.52 50.48	1.66	1.19	0.040
BD (1)C3-H351.9781	σ	62.42 37.58	BD* (1)C2-N20 0.02675	σ*	62.16 37.84	0.99	0.83	0.026
BD (1)C3-H351.9781	σ	62.42 37.58	BD* (1)C2-H34 0.02504	σ*	36.22 63.78	1.59	0.95	0.035
BD (1)C3-C41.97615	σ	49.43 50.57	BD* (1)C4-H32 0.01562	σ*	37.46 62.54	2.50	0.95	0.043
BD(1) C4-C5 1.97741	σ	50.48 49.52	BD* (1)C3-C4 0.02430		50.57 49.43	0.71	1.01	0.024
BD (1)C4-C5 1.97741	σ	50.48 49.52	BD* (1)C3-O11 0.02483	σ*	66.47 33.53	1.90	0.93	0.037
BD (1)C4-C5 1.97741	σ	50.48 49.52	BD* (1)C4-H32 0.01562	σ*	37.46 62.54	0.63	1.07	0.023
BD (1)C4-C5 1.97741	σ	50.48 49.52	BD* (1)C4-H36 0.01235	σ*	37.45 62.55	0.80	1.07	0.026
BD (1)C4-C5 1.97741	σ	50.48 49.52	BD* (1)C5-C6 0.12449	σ*	46.42 53.58	0.57	0.96	0.021
BD (1)C4-C5 1.97741	σ	50.48 49.52	BD* (1)C6-O7 0.05312	σ*	66.38 33.62	1.21	1.19	0.034
BD (1)C4-C5 1.97741	σ	50.48 49.52	BD* (1)O9-H10 0.05186	σ*	22.85 77.15	1.69	1.06	0.038
BD (1)C4-H32 1.97573	σ	62.54 37.46	BD* (1)C3-O11 0.02483	σ*	66.47 33.53	1.17	0.79	0.027
BD (1)C4-H32 1.97573	σ	62.54 37.46	BD* (1)C3-H35 0.03385	σ*	37.58 62.42	2.25	0.95	0.041
BD (1)C4-H32 1.97573	σ	62.54 37.46	BD* (1)C5-C6 0.012449	σ*	46.42 53.58	4.12	0.82	0.052

BD (1)C4-H32 1.97573	σ	62.54 37.46	BD* (1)C5-O9 0.03764	σ*	66.92 33.08	0.72	0.84	0.022
BD (1)C4-H32 1.97573	σ	62.54 37.46	BD* (1)C5-O28 0.10041	σ*	69.96 30.04	0.55	0.74	0.018
BD (1)C4-H36 1.97433	σ	62.55 37.45	BD* (1)C2-C3 0.04675	σ*	47.83 52.17	3.46	0.85	0.048
BD (1)C4-H36 1.97433	σ	62.55 37.45	BD* (1)C5-O28 0.10041	σ*	69.96 30.04	4.41	0.75	0.051
BD (1)C5-C6 1.98220	σ	53.58 46.42	BD* (1)C4-C5 0.03863	σ*	49.52 50.48	0.60	1.00	0.022
BD (1)C5-C6 1.98220	σ	53.58 46.42	BD* (1)C4-H32 0.01562	σ*	37.46 62.54	1.47	1.05	0.035
BD (1)C5-O9 1.99130	σ	33.08 66.92	BD* (1)C1-O28 0.02939	σ*	67.26 32.74	1.30	1.17	0.035
BD (1)C5-O9 1.99130	σ	33.08 66.92	BD* (1)C3-C4 0.02430		50.57 49.43	1.48	1.25	0.039
BD (1)C5-O9 1.99130	σ	33.08 66.92	BD* (1)C6-O8 0.5474	π*	66.80 33.20	1.32	1.43	0.039
BD (1)C5-O28	σ	30.04 69.96	BD* (1)C1-C13 0.03877	σ*	49.68 50.32	1.47	1.14	0.036
BD (1)C5-O28	σ	30.04 69.96	BD* (1)C4-H36 0.01235	σ*	37.45 62.55	1.52	1.22	0.038
BD (1)C5-O28	σ	30.04 69.96	BD* (1)C6-O7 0.05312	σ*	66.38 33.62	1.87	0.80	0.034
BD (1)C6-O7	σ	33.62 66.38	BD* (1)C4-C5 0.03863	σ*	49.52 50.48	0.83	1.38	0.030
BD (1)C6-O7	σ	33.62 66.38	BD* (1)C6-O8 0.5474	π*	66.80 33.20	0.58	1.55	0.027
BD (2)C6-O7 1.98649	σ	25.54 74.46	BD* (1)C5-O28 0.10041	σ*	69.96 30.04	2.87	0.60	0.037
BD (2)C6-O7 1.98649	σ	25.54 74.46	BD* (2)C6-O7 0.37035	σ*	74.46 25.54	2.12	0.37	0.025
BD (1)C6-O8 1.99521	σ	33.20 66.80	BD* (1)C5-O9 0.03764	σ*	66.92 33.08	0.53	1.33	0.024
BD (1)C6-O8 1.99521	π	33.20 66.80	BD* (1)C6-O7 0.05312	σ*	66.38 33.62	0.63	1.55	0.029
BD (1)O9-H10	σ	77.15 22.85	BD* (1)C4-C5 0.03863	σ*	49.52 50.48	3.63	1.08	0.056
BD (1)O9-H10	σ	77.15 22.85	BD* (1)C4-C5 0.03863	σ*	49.52 50.48	1.20	1.03	0.031
BD (1)O11-H12 1.98865	σ	76.42 23.58	BD* (1)C3-C4 0.02430	σ*	50.57 49.43	2.71	1.10	0.049
BD (1)C13-C14	σ	49.78	BD* (1)C1-C2 0.03956	σ*	50.72	1.91	0.97	0.038

1.97994		50.22			49.28			
BD (1)C13-C14 1.97994	σ	49.78 50.22	BD* (1)C1-C13 0.03877	σ*	49.68 50.32	0.63	0.98	0.023
BD (1)C13-C14 1.97994	σ	49.78 50.22	BD*(1)C13-H39 0.02518	σ*	37.97 62.03	0.70	1.06	0.024
BD (1)C13-C14 1.97994	σ	49.78 50.22	BD*(1)C14-H31 0.02469	σ*	37.83 62.17	0.61	1.07	0.023
BD (1)C13-C14 1.97994	σ	49.78 50.22	BD*(1)C15-O17 0.01063	σ*	66.72 33.28	2.03	0.93	0.039
BD (1)C13-C14 1.97994	σ	49.78 50.22	BD*(1)O16-H18 0.04241	σ*	21.87 78.13	0.76	1.07	0.025
BD (1)C13-O37 1.99063	σ	33.17 66.83	BD* (1)C1-H33 0.03884	σ*	38.27 61.73	1.15	1.28	0.034
BD (1)C13-O37 1.99063	σ	33.17 66.83	BD*(1)C14-O16 0.03030	σ*	68.04 31.96	2.16	1.09	0.043
BD (1)C13-H391.97309	σ	62.03 37.97	BD* (1)C1-O28 0.2939	σ*	67.26 32.74	3.46	0.81	0.047
BD (1)C13-H391.97309	σ	62.03 37.97	BD*(1)C14-H31 0.02469	σ*	37.83 62.17	2.38	0.97	0.043
BD (1)C13-H391.97309	σ	62.03 37.97	BD*(1)O37-H38 0.02238	σ*	24.44 75.56	2.16	0.96	0.041
BD (1)C14-C151.98628	σ	50.80 49.20	BD* (1)C1-C13 0.03877	σ*	49.68 50.32	2.26	0.97	0.42
BD (1)C14-O161.99116	σ	31.96 68.04	BD*(1)C13-O37 0.2052	σ*	66.83 33.17	1.55	1.10	0.037
BD (1)C14-H311.97902	σ	62.17 37.83	BD*(1)C13-H39 0.02518	σ*	37.97 62.03	2.49	0.96	0.044
BD (1)C15-O171.99523	σ	33.28 66.72	BD*(1)C13-C14 0.04624	σ*	50.22 49.78	1.45	1.16	0.037
BD (1)C15-H291.98864	σ	60.19 39.81	BD*(1)C14-H31 0.02469	σ*	37.83 62.17	2.36	0.95	0.042
BD (1)C15-H30	σ	61.72 38.28	BD*(1)C14-O16 0.03030	σ*	68.04 31.96	3.86	0.78	0.049
BD (1)C15-H30	σ	61.72 38.28	BD*(1)O17-H19 0.02204	σ*	25.14 74.86	2.35	0.96	0.042
BD (1)N20-H211.97752	σ	73.59 26.41	BD* (1)C2-H34 0.02504	σ*	36.22 63.78	1.28	1.12	0.034
BD (1)N20-H211.97752	σ	73.59 26.41	BD*(1)C22-O23 0.04451	π*	65.90 34.10	4.00	1.17	0.061

BD (1)N20-H211.97752	σ	73.59 26.41	BD*(2)C22-O23 0.29952	π*	71.71 28.29	2.74	0.69	0.039
BD (1)C24-H251.98585	σ	62.84 37.16	BD*(1)C22-O23 0.04451	π*	65.90 34.10	2.87	1.06	0.049
BD (1)C24-H251.98585	σ	62.84 37.16	BD*(2)C22-O23 0.29952	π*	71.71 28.29	3.40	0.58	0.040
BD (1)C24-H261.97519	σ	62.39 37.61	BD*(1)C22-O23 0.04451	π*	65.90 34.10	1.11	1.05	0.031
BD (1)C24-H261.97519	σ	62.39 37.61	BD*(2)C22-O23 0.29952	π*	71.71 28.29	4.51	0.57	0.045
BD (1)C24-H271.98594	σ	62.39 37.61	BD* (1)N20-C22	σ*	37.50 62.50	3.51	1.02	0.054

Table S2: FT-IR, Raman activity, Vibrational bonds, and their assignment for SA and Galactose with different Frequency.

Frequency cm^{-1}	**Observed bands**	**Vibrational Bond (SA)**	**Assignments (SA)**	**Vibrational Bond (Galactose)**	**Assignments (Galactose)**
3483	385^{IR}	H(21)-N(20)	Antisymmetric	H(62)-O(61)	Rocking
3352	649^{IR}	H(21)-N(20)	Rocking	H(62)-O(61)-C(59)	Rocking
1597	258^{IR}	C(22)-N(22)-H(21)	antisymmetric	H(62)-O(61)	Rocking
1497	179^{IR}	C(14)-O(16)-O(18)	Rocking	C(55)-O(57)-H(58)	Scissoring
1474	52^{R}	C(14)-O(16)-O(18)	Rocking	C(55)-O(57)-H(58)	Scissoring
1470	21^{R}	C(14)-O(16)-O(18)	Rocking	C(55)-O(57)-H(58)	Scissoring
1444	87^{IR}	H(18)-O(16)-C(14)	Rocking	C(55)-H(56)	antisymmetric
1434	33^{IR}	H(18)-O(16)-C(14)	Rocking	C(51)-C(55)-H(56)	Scissoring
1422	87^{R}	H(34)-C(2)-N(20)	Rocking	H(62)-O(61)-C(59)	Scissoring
1416	22^{R}	C(4)-C(2)-N(20)	Antisymmetric	C(40)-C(59)	Rocking
1412	59^{IR}	H(21)-N(20)-C(22)	Rocking	C(59)-O(61)-H(62)	Rocking
1377	8^{IR}	H(18)-O(16)-C(14)	Rocking	H(58)-O(57)-C(55)	Rocking

1357	100^{IR}	H(18)-O(16)-C(14)	Rocking	H(58)-O(57)-C(55)	Rocking
1352	100^{IR}	O(16)-C(14)	antisymmetric	H(58)-O(57)-C(55)	Rocking
1346	33^{IR}	C(24)-C(22)-N(20)	antisymmetric	O(61)-H(62)	antisymmetric
1337	35^{R}	H(18)-O(16)	Antisymmetric	H(58)-O(57)-C(55)	Rocking
1328	39^{IR}	C(22)-N(20)-H(21)	Antisymmetric	H(58)-O(57)-C(55)	Rocking
1318	105^{R}	C(22)-N(20)-H(21)	Rocking	H(62)-O(61)-C(59)	Rocking
1307	75^{R}	C(22)-N(20)-H(21)	Antisymmetric	H(62)-O(61)-C(59)	Rocking
1287	21^{R}	C(2)-N(20)	Rocking	H(62)-O(61)-C(59)	Rocking
1270	20^{IR}	C(2)-N(20)	Rocking	H(62)-O(61)-C(59)	Rocking
1244	29^{R}	C(2)-N(20)-H(21)	Antisymmetric	H(62)-O(61)-C(59)	Rocking
1238	30^{IR}	C(2)-N(20)-H(21)	Rocking	H(62)-O(61)-C(59)	Rocking
1230	23^{IR}	H(31)-C(14)-O(16)	Scissoring	C(55)-O(57)-H(58)	Rocking
1227	28^{IR}	O(11)-N(20)-H(21)	Rocking	O(61)-C(59)	Rocking
1167	52^{IR}	C(2)-N(20)-H(21)	Rocking	H(62)-O(61)-C(59)	Rocking
1149	28^{IR}	H(33)-C(1)-C(2)	Scissoring	H(63)-C(59)-O(61)	Scissoring
1142	11^{R}	C(14)-C(13)-C(1)	Scissoring	H(58)-O(57)-C(57)	Rocking
1124	30^{IR}	N(20)-C(5)-C(1)	Antisymmetric	C(40)-C(59)	Antisymmetric
1118	51^{IR}	C(5)-C(1)	Antisymmetric	C(59)-O(61)	Antisymmetric
1109	340^{IR}	N(20)-C(5)-C(1)	Antisymmetric	C(40)-C(59)-O(61)	Antisymmetric
1102	59^{IR}	N(20)-C(2)-C(1)	antisymmetric	C(40)-O(42)	antisymmetric
1099	29^{IR}	C(22)-C(24)-H(24)	Scissoring	C(40)-C(59)-O(61)	Antisymmetric
1081	79^{IR}	C(22)-C(24)-H(27)	Scissoring	H(41)-C(40)-O(42)	Rocking
1078	53^{IR}	O(16)-C(14)-C13	Antisymmetric	H(58)-O(57)-C(56)	Rocking
1068	53^{IR}	C(24)-C(22)	Antisymmetric	H(52)-C(55)-H(56)	Rocking
1046	119^{IR}	C(2)-N(20)-H(21)	Rocking	H(56)-C(55)-C(51)	Rocking
1042	57^{IR}	H(26)-C(24)-H(25)	Rocking	O(61)-C(59)-H(60)	Rocking
955	14^{IR}	O(23)-C(22)-N(20)	Scissoring	O(61)-C(59)-H(63)	Rocking
930	48^{IR}	N(20)-C(2)-C(3)	Rocking	O(61)-C(59)-H(40)	Twisting
830	22^{IR}	C(2)-N(20)-H(21)	Scissoring	H(62)-O(61)-C(59)	Rocking
799	24^{IR}	C(2)-N(20)-H(21)	Rocking	H(62)-O(61)-C(59)	Twisting
787	103^{IR}	C(5)-C(6)-H(21)	Rocking	H(62)-O(61)-C(59)	Rocking
748	63^{IR}	N(20)-H(21)	Antisymmetric	O(61)-H(62)	antisymmetric
747	106^{IR}	C(2)-N(20)-H(21)	Rocking	H(41)-C(40)-C(55)	Rocking

		C(14)-O(16)	Antisymmetric	-	-
699	11^{R}	N(20)-H(21)	Antisymmetric	C(40)-C(55)	antisymmetric
625	30^{R}	O(11)-H(12)	Antisymmetric	C(43)-C(47)	antisymmetric
552	106^{IR}	C(15)-C(14)-C(16)	Rocking	H(58)-O(57)-C(55)	Rocking
526	49^{R}	H(19)-O(17)-O(15)	Rocking	O(47)-C(43)-C(47)	Scissoring
438	10^{R}	O(11)-C(3)-C(2)	Rocking	C(59)-C(40)-O(42)	Rocking
305	15^{IR}	N(20)-C(22)-C(24)	Scissoring	C(55)-O(57)-H(58)	Rocking
261	8^{R}	H(34)-C(2)-N(20)	Scissoring	O(61)-C(59)-H(60)	Scissoring
229	20^{IR}	C(4)-C(5)-C(6)	Rocking	O(61)-C(59)-C(40)	Rocking

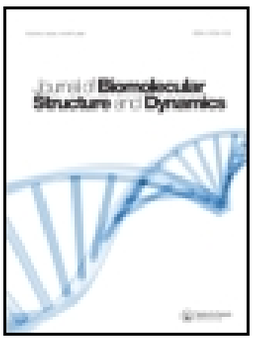

Taylor & Francis
Taylor & Francis Group

Journal of Biomolecular Structure and Dynamics

ISSN: 0739-1102 (Print) 1538-0254 (Online) Journal homepage: https://www.tandfonline.com/loi/tbsd20

Molecular interaction between bi-antennary phenylboronic acid and sialic acid using density functional theory and multi-time scale trajectories

Anjali Patel, Sanjay Tiwari & Prafulla K Jha

To cite this article: Anjali Patel, Sanjay Tiwari & Prafulla K Jha (2019): Molecular interaction between bi-antennary phenylboronic acid and sialic acid using density functional theory and multi-time scale trajectories, Journal of Biomolecular Structure and Dynamics, DOI: 10.1080/07391102.2019.1596839

To link to this article: https://doi.org/10.1080/07391102.2019.1596839

LETTER TO THE EDITOR

Molecular interaction between bi-antennary phenylboronic acid and sialic acid using density functional theory and multi-time scale trajectories

Anjali Patel[1], Sanjay Tiwari[2,*] and Prafulla K Jha[1,*]

[1]Department of Physics, Faculty of Science, The Maharaja Sayajirao University of Baroda, Vadodara- 390 002, Gujarat, India

[2]UKA Tarsadia University, Maliba Pharmacy College, Gopal-Vidyanagar Campus, Surat, 394350, Gujarat, India

[*]Email: tiwarisanju@gmail.com, prafullaj@yahoo.com

Keywords: cancer, hypersialylation, recognition saccharides, density functional theory, targeted theranostics.

Introduction:

Increased expression of sialylated glycans has been correlated to cancer progression, poor prognosis and higher metastatic potential (Dube & Bertozzi, 2005). Studies document functional roles of aberrant sialylation in driving cancer progression at various stages, particularly from the perspective of modulating immune cell responses. It occurs through differential expression of glycosyltransferases, glycosidases and monosaccharide transporters within the cancer microenvironment. Most often, it is implicated aschain-end hypersialylation and increased addition of the non-human sialic acid N-glycolyl-neuraminic acid (Neu5Gc) into cell surface glycans (Pearce & Läubli, 2015). Cancer-associated hypersialylation affects the interaction of tumor cells with sialic acid-binding lectins, particularly those responsible for maintaining the appropriate inflammatory environment (Rodrigues & Macauley, 2018). Development of efficient

methodologies on quantifying SA expression in tissue samples remains attractive, particularly from the standpoints of early detection of cancer. At the same time, SA-specific molecular recognition can be exploited to selectively localize the therapeutic agents in the region highly sialylated epitopes, thereby sparing the healthy cells (Tiwari, 2018).

Interaction between saccharides or saccharide mimetics with SA has been studied using experimental and theoretical approaches (Patel, Tiwari, & Jha, 2018; Tiwari, Tirosh, & Rubinstein, 2017). Boronic acids display the ability to form reversible covalent interactions with SA (Matsumoto, Cabral, Sato, Kataoka, & Miyahara, 2010). Using ^{17}O-NMR studies, Djanashvili and coworkers (2005) demonstrated that phenylboronic acid (PBA) forms esters with SA between pH 2 and 12. At low pH (2–8), the α-hydroxycarboxylate moiety at C1/C2 is involved in the binding, whereas at pH >8 the binding of PBA takes place at the glycerol side chain to give a five-membered ester at C_8 and C_9. Molecular docking studies also supported these results. At physiological pH, carboxyl group acted as negative charge center on the SA molecule and did not participate in the interaction (Djanashvili, Frullano, & Peters, 2005).

SA-PBA complexation is favored by the trigonal form, for which involvement of multiple metastable binding sites along with intra-molecular stabilization via B-N or B-O interactions are crucial. However, experimental evidence suggests high affinity interaction of polyvalent saccharides with SA in cancer cells (David, Kopecková, Kopecek, & Rubinstein, 2002). Our earlier studies showed an enhanced SA-PBA interaction with a shift from mono- to divalent interaction. Binding constant orders of magnitude higher than that of monovalent interaction was observed. Based on quantum mechanical calculations, we concluded that saccharides (mannose and galactose) have high binding affinity for extra-cellular SA, specifically at tumor-relevant pH and temperature conditions (Patel et. al., 2018). Binding can

further be improved through increasing the valency of saccharide ligands (David et al., 2002). With these insights, we here in demonstrate the ability of bi-antennary ligands to achieve a high affinity interaction with the extra-cellular SA on a molecular level. We employ the top scored binding saccharide as input of subsequent MD simulation to provide a biological relevance and trajectory. We present the vibrational spectra, supported by potential energy distribution (PED) analysis. PED analysis of the theoretical spectra forms the basis for the elucidation of the future matrix isolation IR spectra. In the last few decades this type of interaction has been studied extensively using DFT and MD simulation. Recently, a significant conformational difference in the wild-type and ΔK9 form of thrombin is observed using a combined molecular dynamics simulation and machine learning (Xiao, Melvin, & Salsbury, 2018). Jana and coworkers (2018) performed a study to search highly specific, less toxic, non-ZBG inhibitors of MMP-9, on the basis of e-pharmacophore and ligand-based approaches to develop drug for the various disorders.

Computational:

The structure of receptor SA complex with different ligands such as bi-antennary GAL, MAN, and PBA is fully optimized by 6-31G basis set using GAUSSIAN 09 suite (Frisch, Trucks, Schlegel, Scuseria, Robb et. al., 2016). B3LYP (Becke's three parameter hybrid functional using the Lee-Yang-Parr correlation function) (Lee, Yang, & Parr, 1998) was used for obtaining the global energy minimized structure at ground state and density functional theory (DFT) was employed to study the quantum chemical properties such as molecular orbital structure, vibrational frequencies, PED (using VEDA 4 program), atomic charge, electrophilicity [ω], chemical hardness[η], chemical softness[σ] and electro chemical potential[μ] and energy of determined structures with the help of the Koopman's theorem for closed shell molecule (Tsuneda, Song, Suzuki, & Hirao, 2010). The individual molecular structures were placed at a

close distance to relax under zero external stress and ideal unconstrained conditions before using them for any further computations. Ligands are placed nearer to the active side such that the most active site is nearest to the amine group. Interaction energy (E_{int}^{AB}) of ligand target binding was calculated as the difference between the energy of complex and sum of the energies of its total fragments:

$$E_{int}^{AB} = E_{AB}^{opt} - (E_A^{opt} + E_B^{opt}) + E_{AB}^{BSSE} \quad [1]$$

Where, E_{AB}^{opt}, E_A^{opt}, E_B^{opt} and E_{AB}^{BSSE} are complex energy, ligand energy, receptor energy and basis set superposition error respectively. Details of these calculations are described in our earlier work (Patel et al., 2018).

Molecular dynamics (MD) simulation:

Full atom MD simulation was performed for the considered system. Initial minimization was done using steepest descent and conjugate gradient method. The minimized system was pulled in to the solution of TIP3P water molecules with orthorhombic periodic boundary condition. The optimized complex was subjected to heating to 300K over 1.2ns simulation time for NVT ensemble at Berendsen barostat and 5ns, 15ns and 25ns of simulation time for NPT ensemble at Nose-Hoover thermostat. Approximately 500 frames were retrieved along the coordinates for all NPT simulation times. Interval trajectory length for 5ns, 15ns and 25ns simulations are10ps 30ps and 50ps with 1 bar pressure and 300K temperature. Root mean square deviation (RMSD) calculated for last frames of three simulations were compared. We adopted the OPLS_2005 force fields (Banks, Beard, Cao, Cho & Damm, 2005). The deviation in shape is quantified via the RMSD at time t500 with respect to a given reference structure at time t1:

$$\text{RMSD (t1, t2)} = \sum_{Ni=1}^{N} (Xi(t2) - Xi(t1))1/2 \quad [2]$$

Xi (t) is position of atom i at time t and N is the total number of atom in the molecules. The first frame of trajectory (t1) is used as a reference and values of the RMSD.

Results and Discussion:

We employed the MD simulations combined with QM (DFT)/MM calculations to understand the PBA-SA interaction. This interaction depends on the inter-atomic channel of 3D molecular structure (Figure 1). While receptor binds competitively and comparably with high affinity to bi-antennary Gal, Man, and PBA, they elicit different biological activities and expose the content of highly SA loaded cell suggesting that there are auxiliary functions to express the tumor cells. Bi-antennary PBA domain is the primary region of interest for probing the impact of SA activators, and binding affinities of this ligand to cellular SA domain. The binding of three complexes have been compared amongst themselves. These receptor-ligand complexes were simulated in various time slots and analyzed with VMD-1.9.2 and GAUSSIAN-09 which reveals that the hydrogen bonding is taking place in the reaction.

Optimization of bi-antennary systems and SA:

Distance between two molecules corresponding to the optimized geometry of complexes have been obtained using the DFT method and presented in Table 1. In addition, it presents the parameters associated with the optimized geometry of complexes with single antennary galactose obtained in our previous study (Patel et. al., 2018).

The data clearly depict that the bond distance is minimum for bi-antennary PBA. These are also supported from the binding energy values presented in same table. This is remarkable in context of single antennary where the bond length for best binding configuration is of this range. The

experimental study of David and group also supports our finding that the bi-antennary PBA binds SA strongly.

This complex attributed to the fact that the bi-antennary galactose is highly flexible due to hydrophobic spacer arms that allow variation of their intergalactic distance and geometries which confirms the interaction between oligomeric structure and galactose.

Molecular dynamics simulation:

RMSD plots shows that the proposed saccharides (bi-antennary Gal, Man and PBA) worked as good inhibitors, where bi-antennary PBA expressed as competitive inhibitors against SA (Figure 2). Each panel shows representative plots (for the reason of conciseness, results 1 and 500 trajectories are displayed) of RMSD values obtained between configurations of one MD trajectory separated by respective time lags (X- axis). With an increase in the time-lag between configurations, fluctuation in the RMSD values can be noticed. We note that for all multiple time duration SA and 2PBA remained stable as shown using RMSD plots (Figure 2(a-c)). In principle less RMSD value shows high stability and ground state energy. The time course of the SA-ligand interaction (5, 15 and 25 ns) is presented Table 2. It shows minor deviation sat these time scales; the values range from 7.12 to 15.46Å. Here 25ns is not highly stable so we can say 15ns and 5ns configuration are the best poses for further process accordingly. Moreover, most of the dimers grow during the simulation times.

Frontier Molecular Orbital analysis:

HOMO (Highest Occupied Molecular Orbital) is known as the ability of a molecule to donate while LUMO (Lowest Unoccupied Molecular Orbital) represents the ability to obtain electron recognized as frontier molecular orbital. They play a key role in computing optical and electronic properties of a molecule (Figure 3). Less energy gap is conductive to higher charge transfer potential inside the

receptor and it is related to higher interaction energy. In mono-antennary configuration, the band gap for PBA and Gal was found as 0.0511and 0.0289 eV, respectively (see Table 1).

Corresponding values for bi-antennary PBA and GAL were found to be 0.1559 and 0.2046 eV, respectively. This is due to the biological environment which we have provided

during our simulations. The HOMO of π nature is localized over the C=O bond. By contrast, the LUMO is located over 2PBA (i.e. benzene ring). These observations lead us to the conclusion that the bi-antennary configuration is highly conducting than the single antennary (Patel et. al., 2018).

Above figure shows the difference between band gap before and after simulation for a specific time slot. While, structure after 15ns simulation appears highly conducting due to the less band gap about 0.035 eV resulting in to a strong binding as compared to other time dependent structures. The fastest conducting event occurs in around 15ns whereas no apparent effect on time dependent other complex is observed. In the case of hardness and softness, it is controversy with the ideal case. Where, hardness of bi-antennary galactose, mannose and PBA shows 0.078eV, 0.0566eV and 0.102eV respectively and softness are 6.4102eV, 8.8339eV and 4.9019eV respectively (Table 1). Here some external potential is may be present. For different time dependent complexes surface reactivity goes with the flow of binding energy (Table 2). Where, hardness for 5ns, 15ns and 25ns are 0.0260eV, 0.0173eV and 0.0285eV respectively and softness are 19.2307eV, 28.9017eV, 17.5438eV respectively. These gathered data shows the hardness of best binded complex is reduced approx. 33% with 5ns complex and approx. 39% with 25ns complex.

Mulliken charge:

Mulliken population analysis (Mulliken, R.S., 1955) yields a means of estimating partial atomic charge known as Mulliken atomic charge. Even though, Mulliken atomic charge is not inspectable but its relative values yield consequential knowledge as molecular reactivity and various other properties are dependent on it. Single antennary versus bi-antennary glycans differed at the various glycosylation sites even within same glycoprotein. In 5ns system, maximum negative charge has been found on O_{49} (-0.676785) and O_{69} (0.664322) which may be attributed to the sharing of lone pair of electrons with neighboring atom H_{22} (0.4401). The O_{49} which is a highly electron deficient atom is the member of π electron system. In 15ns simulation system, O_{49} (-0.6879) and O_{41} (-0.6839) carry negative charge which may share electron with H_{24} (0.4365) and H_{21} (0.4512). Moreover, in 25ns system most negative charge holder atoms are O_{40} (-0.6045) and O_{55} (-0.5585). The O_{40} is the π electron atom system. The O_{55} may share the electron with H_{21} (0.4287). All hydrogen and nitrogen carries positive and negative charge, respectively. There is largest change of absolute charge in all cases. From H_{24} to C_{35} and O_{47} shows irregular behavior along the simulation. Atom C_{34} carries negative charge (-0.0035eV) in 25ns structure where for 15ns it conduct positive charge (0.07969eV). This change in the negative to positive is consistent with the prediction of electrophilic and nucleophilic sites on the basis of molecular electrostatic potential surface.

Molecular electrostatic potential (MEP) analysis:

Molecular electrostatic potential (MEP) surface is widely used to predict reactive sites of a molecule for the biological recognition studies and hydrogen bonding (Şen, yilmaz, dincer, &

cukurovali, 2015). It illuminates charge distributions in three dimensions. In Figure 5, different colors on MEP represent different values of electrostatic potential at molecule surface. The blue color shows the electron deficient or partially positive, while red color represents the electron rich or negative regions. Yellow and green colors show the slightly electron rich and neutral region, respectively.

The color coding of map ranging from -0.174 to +0.174 a.u., -0.175 to +0.175 a.u., and -0.165 a.u. to +0.165 a.u. of 5ns, 15ns and 25ns respectively for title molecule. It can be seen from Figure 4(a), 4(b) and 4(c) respectively that the negative region is concentrated over C_{38}, O_{39} and O_{40}; over O_{43}, O_{41}, O_{40}, O_{39} and C_{38}; and O_{39}, O_{40}, O_{41} and C_{38}. This indicates the region around C_{38}, O_{39}, O_{40} and O_{41} is most suitable for electrophilic attack. The region around H_{57}, H_{58} and H_{59} is slightly light blue which indicates it as most probable sight for nucleophilic attack. The rest of the molecule is light green indicate the potential between two extremes. The non-red and non-blue corresponding to mediary potential forms the crucial part of MEP which implies that the electronegativity difference in the molecule is not very great.

Binding Energy:

The binding energy of SA with bi-antennary saccharides and mimic is presented in Table 1 which clearly depicts strong binding affinity of bi-antennary saccharides and mimic towards SA than the single antennary saccharides and mimic (Patel et. al. 2018). The present results are consistent with the experimental study (David et. al., 2002). It is to be noted that the mimic as 2PBA show the highest affinity binding than single antennary saccharides (Patel et. al., 2018).

The present calculations on binding energy are without considering biological environment for example water and body temperature. Therefore to have an exact biological environment we

have simulated full complex in the presents of water molecule, body temperature and body pressure. The simulation is only performing for 2PBA and SA based complex and this shows instant binding in the absence of biological environment. We found that the biological environment affects the binding which is consistent with our earlier report (Patel et. al., 2018). The binding energy reduces to -181.25 kcal/mol from -244.94 kcal/mol (≈26%) (Table 2). This can be due to the fact that it does depend the type and number of bound sugar residue per molecule (David et. al., 2002). Here we have mentioned from 5 ns MD simulations only because there were no comparative variations in properties.

Vibrational analysis:

The vibrations are influenced by C-C bonds. These vibrations are within the region 1000 to 1300 cm^{-1} (Gunasekaran, Kumaresan, Arunbalaji, Anand, and Srinivasan, 2008) based on experiments. In the present study, the vibrations (supplementary table) in SA are observed at 1293.71cm^{-1} with rocking C_{33}-C_{45} in IR bands. These results show that the theoretical values are better conformity with experimental data. The N-H stretches of amine group is found in 3000 to 3500 cm^{-1} region (Gunasekaran et. al, 2008). These have been recorded as antisymmetric vibration at 3300 cm^{-1} (N_{52}-H_{53}) region with 152.71 IR intensity and 97% involvement. The O-C vibrations and their derivatives are recorded at 1000-1300 cm^{-1}. We observe rocking vibrations in 5ns structure at 1173.37 cm^{-1} with 657.62 R intensity between O_{39}-C_{38} atoms with 10% involvement. In 15ns structure rocking vibration is observed at 1079.69 $cm^{-1}$with 179 IR intensity between O_{48}-C_{40} and O_{49}-H_{51} atoms with 36% and 56% PED value respectively. The C-C rocking vibration mode got at 1293.71 cm^{-1} frequency with 438 IR intensity between C_{33}-C_{45} atoms and 18% PED value. PED analysis (supplementary data) shows the H_{21}-O_{41} and H_{24}-O_{49} are intra molecular interacting atoms accordingly we can see for the 25ns complex results in supplementary data. Highly

occupied bond is O-H bond. The C-C-C, H-C-H, C-N-C and vibrations are at 1177 cm^{-1}, 3124 $cm^{-1}$and 798.70 cm^{-1} respectively.

Conclusion: In the present study, we have performed the molecular dynamics simulation and density functional theory calculations to study the induced changes in structural, electronic and vibrational properties of Sialic acid with Bi-antennary PBA. We showed that bi-antennary PBA interacted efficiently with upregulated SA residues on cell surface. Our results indicate that in the presence of strong interaction energy, bi-antennary PBA molecules would spontaneously move towards the SA. Binding energy is -181.2479 kcal/mol with 1.579(Å) distance show that bi-antennary PBA quickly interacted with SA (15 ns). Functional information on these interactions can contribute the development of practically useful ligands which can be employed as theranostic tools.

Conflict of interest: Authors report no conflict of interest.

Acknowledgements: Authors acknowledge the Science and Engineering Research Board (SERB), New Delhi, India (ECR/2017/000903 and SB/S2/CMP-005/2013) for financial support. The computations were performed on 'SAYAJI' cluster developed under DST-FIST program at department of Physics, Faculty of Science, The M. S. University of Baroda, Vadodara, Gujarat, India.

References:

Banks, J.L., Beard, H.S., Cao, Y., Cho, A.E., Damm, W., Farid, R.,… Murphy, R. (2005). Integrated modeling program, applied chemical theory (IMPACT). *Journal of computational chemistry, 26(16), 1752-1780,* DOI: 10.1002/jcc.20292.

David, A., Kopeckova, P., Kopecek. J., & Rubinstein, A. (2002) The role of galactose, lactose, and galactose valency in the biorecognition of N-(2-hydroxypropyl) methacrylamide copolymers by human colon adenocarcinoma cells. *Pharmaceutical Research*, 19(8), 1114-1122. DOI: 10.1023/A:1019885807067.

Djanashvili, K., Frullano, L., & Peters, J.A. (2005). Molecular recognition of sialic acid end groups by phenylboronates. *Chemistry–A European Journal*, 11(13), 4010-4018. DOI: 10.1002/chem.200401335.

Dube, D.H. & Bertozzi, C.R. (2005). Glycans in cancer and inflammation—potential for therapeutics and diagnostics. *Nature reviews Drug discovery*, 4(6), 477-488, DOI: 10.1038/nrd1751.

Frisch, M. J., Trucks, G. W., Schlegel, H. B., Scuseria, G. E., Robb, M. A., Cheeseman, J. R., … Fox, D. J. (2016) Gaussian, Inc., Wallingford CT.

Gunasekaran, S., Kumaresan, S., Arunbalaji, R., Anand G., & Srinivasan, S. (2008) Density functional theory study of vibrational spectra and assignment of fundamental modes of dacarbazine, *Journal of Chemical Sciences*, 120(3), 315-324. DOI: 10.1007/s12039-008-0054-8.

Jamróz, M. H. Vibrational Energy Distribution Analysis: VEDA 4, program, Warsaw, 2004.

Jana, S., & Singh, S.K., (2018). Identification of selective MMP-9 inhibitors through multiple e-pharmacophore, ligand-based pharmacophore, molecular docking, and density functional theory approaches. *Journal of Biomolecular Structure and Dynamics*, 9, 1-22. DOI: 10.1080/07391102.2018.1444510.

Lee, C., Yang, W., & Parr, R. G. (1988) Development of the Colle-Salvetti correlationenergy formula into a functional of the electron density. *Physical Review B*, 37(2), 785-789. DOI:10.1103/PhysRevB.37.785.

Matsumoto, A., Cabral, H., Sato, N., Kataoka, K. & Miyahara, Y. (2010). Assessment of tumor metastasis by the direct determination of cell- membrane sialic acid expression. *AngewandteChemie*, 122(32), 5626-5629. DOI: 10.1002/ange.201001220.

Mulliken, R. S. (1955) Electronic population analysis on LCAO-MO molecular wave functions. *Journal of Chemical Physics*, 23(10), 1833-1840. DOI: 10.1063/1.1740588.

Patel, A., Tiwari, S. & Jha, P.K. (2018). Density functional theory based probe of the affinity interaction of saccharide ligands with extra-cellular sialic acid residues. *Journal of Biomolecular Structure and Dynamics*, 1-10. DOI: 10.1080/07391102.2018.1461690.

Pearce, O.M. & Läubli, H., (2015). Sialic acids in cancer biology and immunity. *Glycobiology*, 26(2), 111-128. DOI: 10.1093/glycob/cwv097.

Rodrigues, E., & Macauley, M. (2018). Hypersialylation in cancer: modulation of inflammation and therapeutic opportunities. *Cancers*, *10*(6), 207-226. DOI: 10.3390/cancers10060207.

Şen, f., yilmaz, i., dincer, m., & cukurovali, a. (2015). Structural features of 2-(4, 5-diphenyl-4h-1, 2, 4-triazol-3-yl) thio)-1-(3-methyl-3-phenylcyclobutyl) ethanone: x-ray diffraction and dft calculations. *Journal of the chilean chemical society*, 60(4), 2671-2676. DOI: 10.4067/S0717-97072015000400009.

Tiwari, S. (2018). Mannosylated constructs as a platform for cell-specific delivery of bioactive agents, *Critical Reviews™ in Therapeutic Drug Carrier Systems*, 35(2), 35(2), 157-194. DOI: 10.1615/CritRevTherDrugCarrierSyst.2018020313.

Tiwari, S., Tirosh, B., & Rubinstein, A. (2017) Increasing the affinity of cationized polyacrylamide-paclitaxel nanoparticles towards colon cancer cells by a surface recognition peptide. *International Journal of Pharmaceutics*, 531(1), 281-291. DOI:10.1016/j.ijpharm.2017.08.092.

Tsuneda, T., Song, J.W., Suzuki, S. & Hirao, K. (2010). On Koopmans' theorem in density functional theory. *The Journal of chemical physics*, 133(17), p.174101. DOI: 10.1063/1.3491272.

Xiao, J., Melvin, R.L., & Salsbury Jr, F.R., (2018). Probing light chain mutation effects on thrombin via molecular dynamics simulations and machine learning. *Journal of Biomolecular Structure and Dynamics*, 1-18. DOI: 10.1080/07391102.2018.1445032.

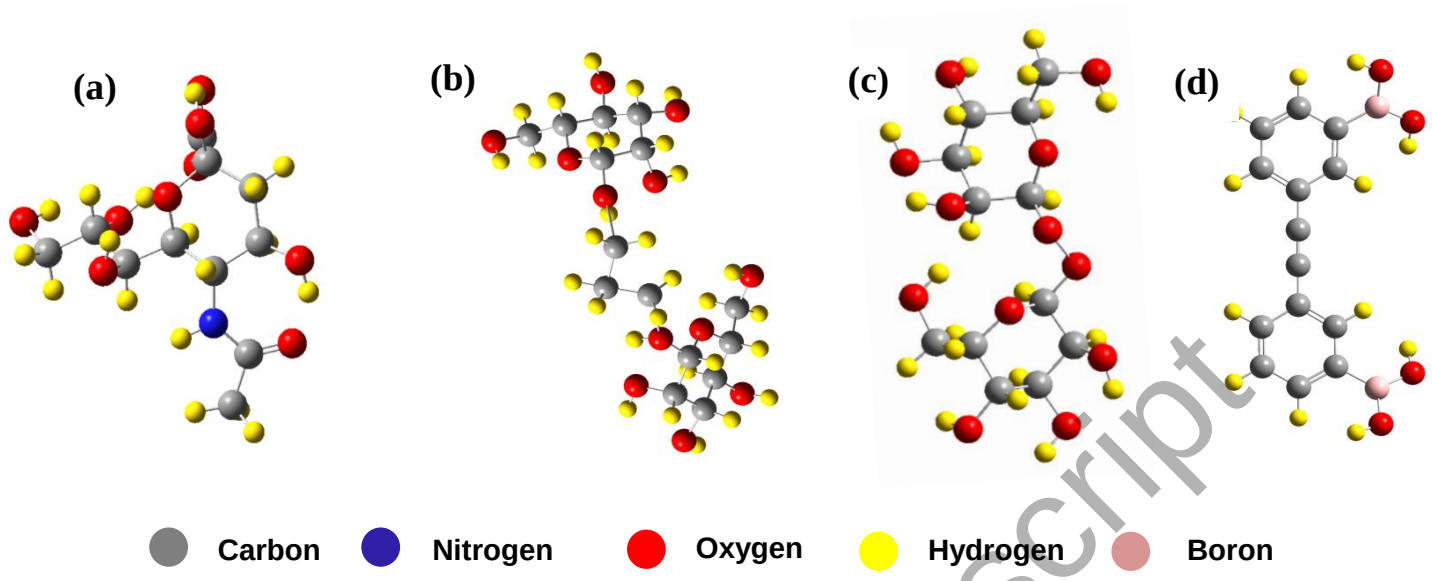

Figure 1: Molecular configuration of sialic acid (a), biantennary Gal (b), biantennary Man (c) and biantennary PBA (d).

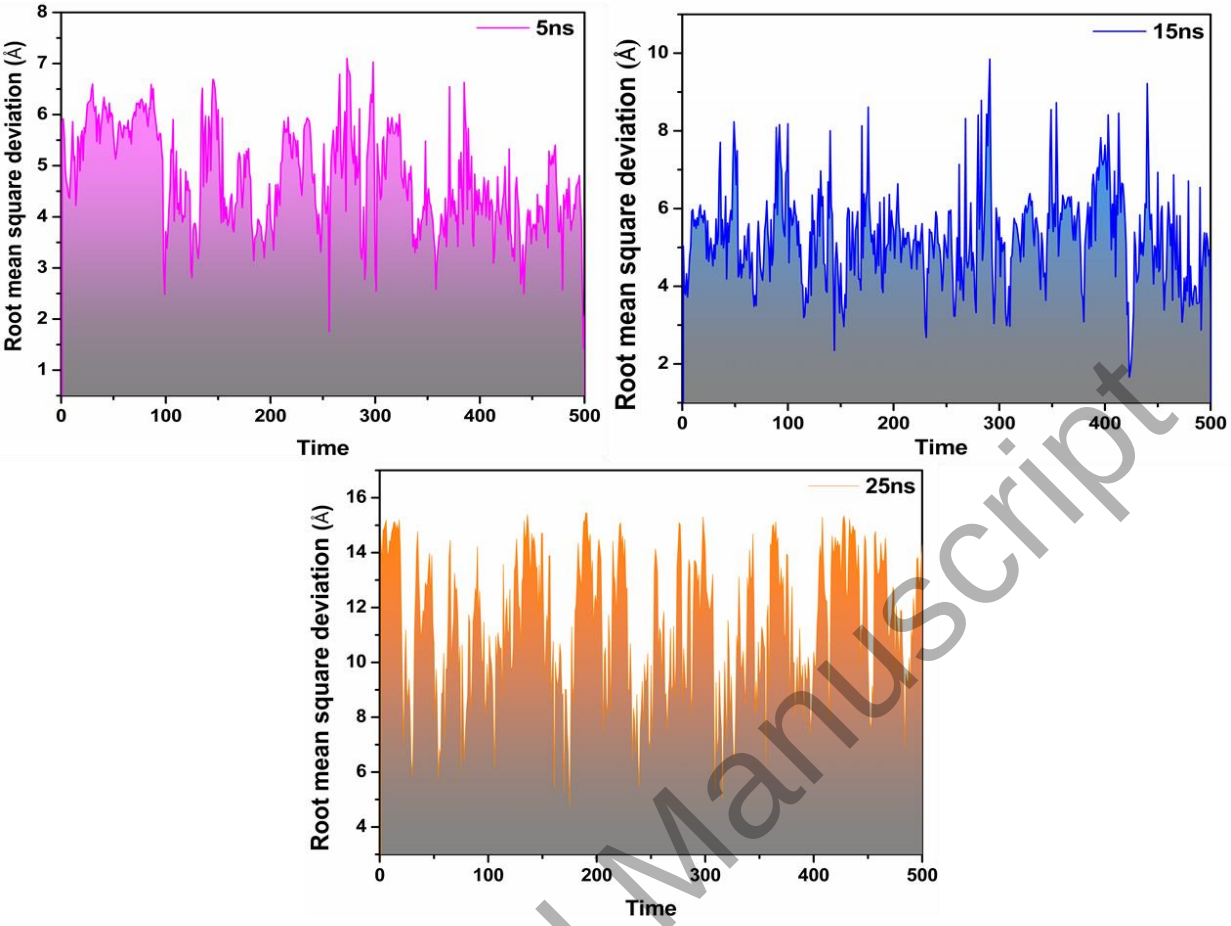

Figure 2: Time course of the root mean square deviation (RMSD) for MD simulations of 5ns (pink) 15ns (blue) and 25ns (orange) of SA with Bi-antennary PBA. The RMSD of 25ns is very high than 5ns and 15ns.

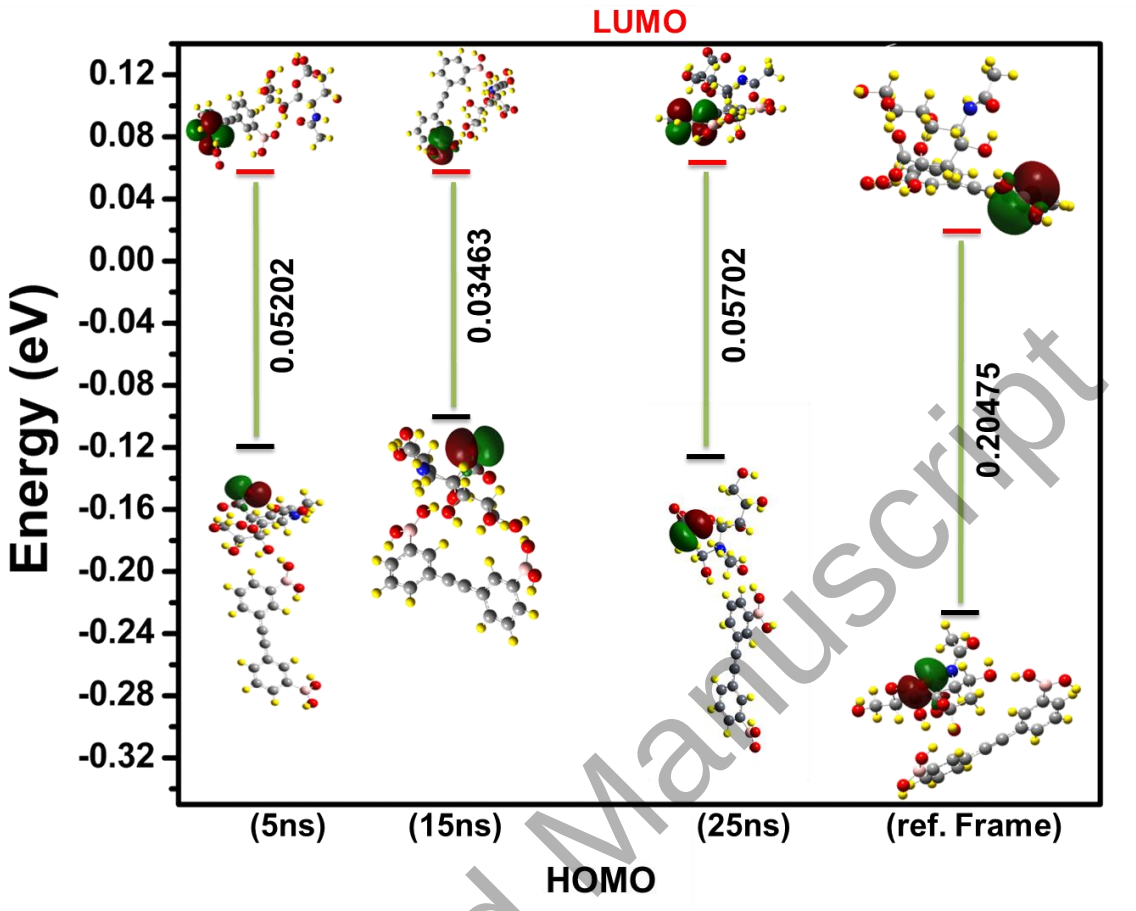

Figure 3: Atomic orbital HOMO and LUMO composition of frontier molecular orbital for 5ns, 15ns and 25ns complex frames of SA-Bi-antennary PBA.

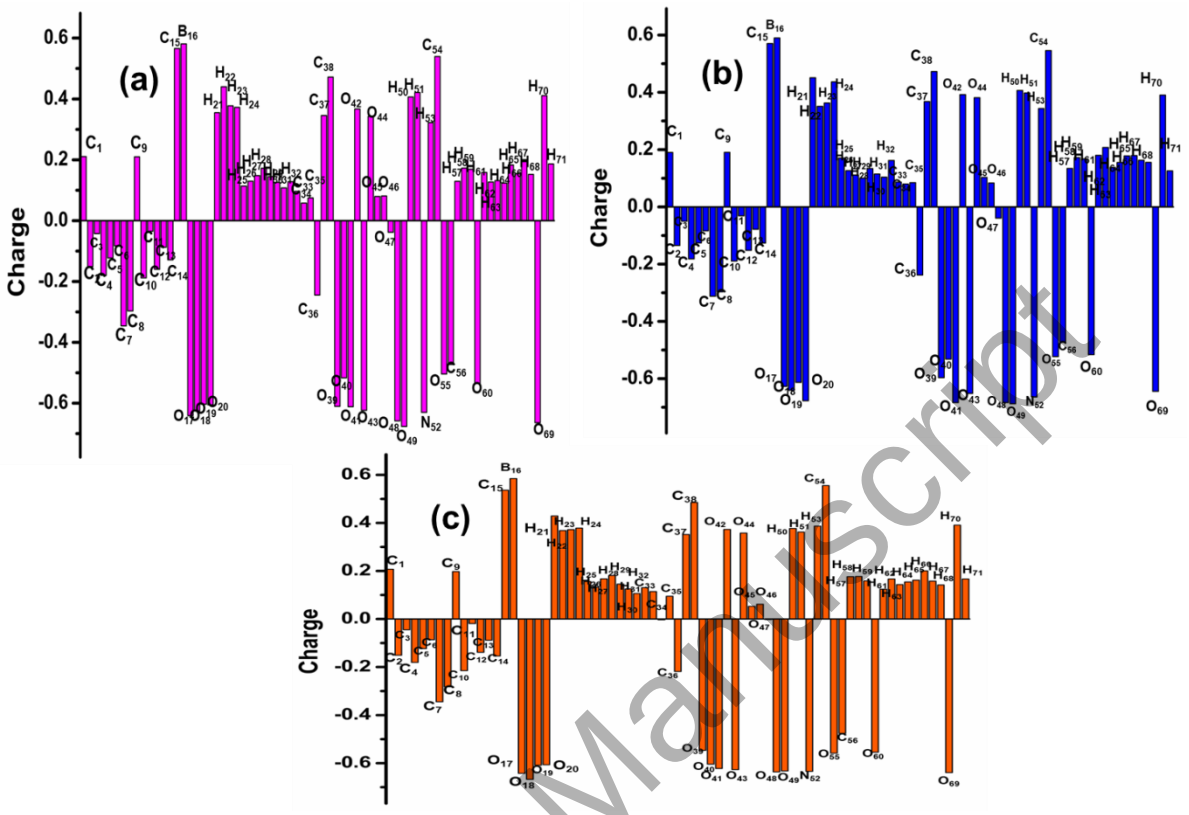

Figure 4: Mulliken charge of (a) 5ns (b) 15ns and (c) 25ns complex frames of SA-Bi-antennary PBA.

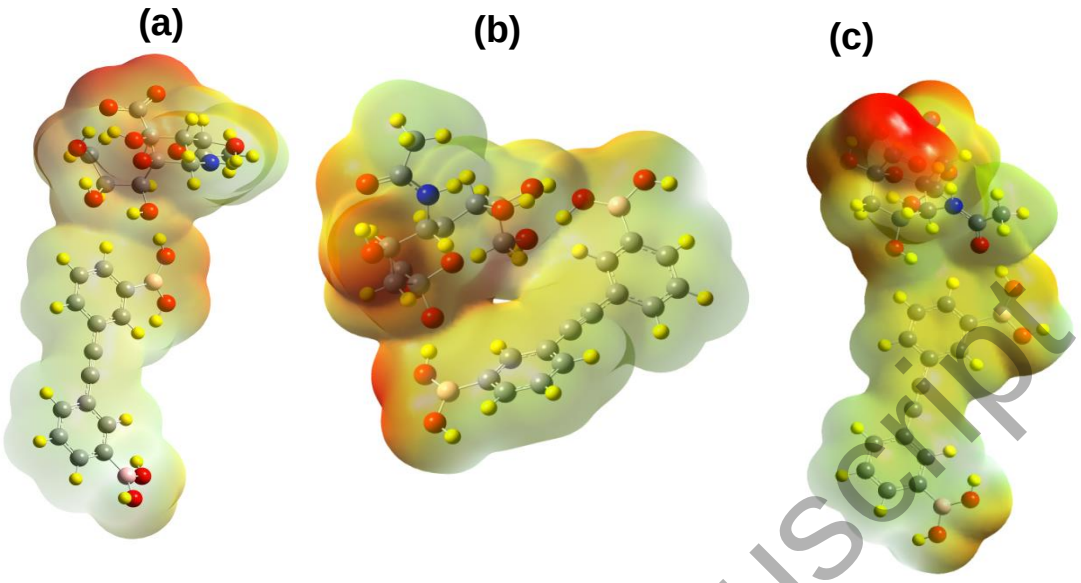

Figure 5. MEP of (a) 5ns (b) 15ns (c) 25ns complex of SA-Bi-antennary PBA.

Table 1: Value of Binding energy, HOMO, LUMO, band gap, Hardness, Softness, Chemical potential, Electrophilicity. Values mentioned in brackets represent the interaction of SA with monovalent saccharides (Patel et al., 2018).

Properties	**SA + Bi-antennary Galactose**	**SA + Bi-antennary Mannose**	**SA + Bi-antennary PBA**
$E_{binding}$(kcal/mol)	49.8781 (-31.7353)	-54.9871 (-23.8794)	-244.9476 (164.4198)
HOMO	-0.1926 (-0.1242)	-0.1529 (-0.1235)	-0.2254 (-0.1083)
LUMO	-0.0366 (-0.0953)	-0.0396 (-0.0667)	-0.0207 (0.0572)
HLG	0.1559 (0.0289)	0.1926 (0.0568)	0.2046 (0.0511)
Distance (Å)	2.74	2.47	1.80
Hardness (η)(eV)	0.078	0.0566	0.102
Softness (σ)(eV)	6.4102	8.8339	4.9019
Chemical Potential (μ)(eV)	0.1146	0.0962	0.12305
Electrophilicity (ω)(eV)	0.084186	0.0081	0.0742

Table 2: Value of Binding, Hardness, Softness, Chemical potential and Electrophilicity for 5ns, 15ns and 25ns complex of SA with Bi-antennary PBA.

Properties	**5ns**	**15ns**	**25ns**
$E_{binding}$(kcal/mol)	-176.4236	-181.2479	-175.4472
Distance (Å)	1.6278	1.579	1.6348
Hardness (η) (eV)	0.0260	0.0173	0.0285
Softness (σ) (eV)	19.2307	28.9017	17.5438
Chemical potential (μ) (eV)	0.08848	0.08871	0.09299
Electrophilicity (ω) (eV)	0.15055	0.22744	0.15170
RMSD (Å)	7.12	9.84	15.46